FACULDADE DE ENGENHARIA DA UNIVERSIDADE DO PORTO

Design of a device to evaluate the friction of safety footwear according to DIN 51130:2014-02

Francisca Guerra Pereira

Master's in Mechanical Engineering

Supervisor: Mário Augusto Pires Vaz

Second Supervisor: Nuno Viriato Marques Ramos

August 4, 2022

Design of a device to evaluate the friction of safety footwear according to DIN 51130:2014-02

Francisca Guerra Pereira

Master's in Mechanical Engineering

August 4, 2022

Abstract

A correct evaluation of the functional properties of floors is fundamental to diminish the risk of slips and falls.

The friction between safety shoes and the floor, measured through the coefficient of friction, is a determining factor for the evaluation of the level of safety that the floor provides. However, this value is not intrinsic to the floor, it varies with the presence of a contaminant and with the type of shoe being worn. Therefore, it is not surprising that, over the last decades, numerous studies have been carried out on various equipment for measuring the friction of certain floors when there are contaminants including water, soapy water or motor oil. Some of these tests have also looked at the effect of the shoe tread pattern.

In this sense, the present work has the objective of on the one hand, making a review of the equipment used for the measurement of friction between flat surfaces (floor and shoe) and on the other hand, to design an equipment capable of carrying out these measurements, according to DIN 51130:2014-02.

The structural calculations performed show both at the static and dynamic level that the system works and can, in the future, be built and used to perform the intended tests.

Keywords: Coefficient of Friction Measurement,Device, Slip and Falls

Resumo

Uma avaliação correcta das propriedades funcionais dos pisos é fundamental para reduzir o risco de escorregamentos e quedas.

O atrito entre o calçado de segurança e o pavimento, medido através do coeficiente de atrito, é um factor determinante para a avaliação do nível de segurança que o pavimento proporciona. No entanto, este valor não é intrínseco ao piso, varia com a presença de um contaminante e com o tipo de calçado que está a ser usado. Por conseguinte, não é surpreendente que, nas últimas décadas, tenham sido realizados numerosos estudos sobre vários equipamentos para medir o atrito de certos pavimentos na presença de contaminantes como a água, água com sabão e óleo. Alguns destes testes também analisaram o efeito do padrão da sola do sapato.

Neste sentido, o presente trabalho tem como objectivo, por um lado, fazer uma revisão do equipamento utilizado para a medição do atrito entre superfícies (chão e calçado) e, por outro, desenvolver o projeto de um equipamento capaz de realizar estas medições, de acordo com a norma DIN 51130:2014-02.

Os cálculos estruturais realizados mostram que, tanto a nível estático como dinâmico, o sistema funciona e pode, no futuro, ser construído e utilizado para realizar os testes pretendidos.

Palavras-Chave: Dispositivo, Medição do Coeficiente de Atrito, Quedas

Acknowledgements

The realization of this project would not have been possible without the contribution of several people, so I would like to express my gratitude:

To my supervisor and cosupervisor, Professor Mário Vaz, and Engineer Nuno Viriato, for all the support given in the execution of this work, especially the availability shown in the clarification of doubts and for the knowledge that was shared throughout the whole process.

To Professor Francisco Queirós de Melo, for all the support, and availability and for sharing stories that made this experience more enriching.

To the LOME engineers, Behzad Farahani, Job Silva and Rogério Lopes, for their help in the realization of this project.

To my coursemates, who in one way or another were part of my academic journey, making it more remarkable.

To my dissertation companions, Mário Oliveira and Jorge Madureira, who accompanied me daily during the dissertation and motivated me to continue when everything seemed to be going wrong.

To my friends, for sharing stories, moments, and frustrations throughout these five years. Without you, it wouldn't have been half as fun.

Finally, my deep and sincere gratitude to my parents and brother for their continuous and unparalleled love, help, and support. I am grateful to my brother for always being there to make me laugh. I am forever indebted to my parents for giving me the opportunities and experiences that have made me who I am.

Francisca Guerra

“Where there’s a will
there’s a way.”

George Herbert

Contents

List of Figures

List of Tables

Abbreviations

ACOF	Available Coefficient of Friction
COF	Coefficient of Friction
CTIOA	Ceramic Tile Institute of America
HSE	Health and Safety Executive
KCOF	Kinetic Coefficient of Friction
PPE	Personal Protective Equipment
RCOF	Required Coefficient of Friction

Chapter 1

Introduction

1.1 Context and Motivation

Falls are caused by a combination of environmental and human factors. Walking surfaces, shoes, pollutants, heights, inclination, and lighting are all environmental considerations to account for. Sensory abilities, biomechanics, neuromuscular control, and information processing are all human factors. Most falls are caused by an individual's incapacity to adjust to changes of the surroundings. If the biomechanics of gait are not adjusted, increasing the slipperiness of a floor surface would result in a greater chance of slipping and falling. In order to prevent slippage, friction must be used to counterbalance the shear forces generated during gait. Whenever the available friction between the shoe and the floor is insufficient to fulfill the biomechanical demands, a slip is likely to occur, potentially resulting in injury.

The slip resistance of the shoe's surface contact with the ground is considered the most important environmental element in falls. A low friction level on the shoe-floor interface can lead to a lack of traction, which can cause a slip and eventually a fall. However, a misstep that does not result in a fall can also lead to injury because even if stability is regained after a slip, injuries can still occur as a result of contacting an object or a muscular tension [1].

One of the most frequent causes of fatal and non-fatal workplace injuries is slips and falls due to slick conditions [2] and 90% of these accidents are due to wet floors, according to the Health and Safety Executive (HSE) [3].

In 2019, trips and falls accounted for 15.50% of reported occupational injuries and 21.15% of deaths among Portuguese citizens [4]. Since these types of events are so recurrent, they are the biggest cause of worker's compensation claims and days away from work [5]. Thus, preventing them will reduce these events [6]. It should be noted that these values do not include injuries caused by slipping and recovery and are therefore underestimated, which means that the number of injuries due to this type of event is much higher than reported [1].

Therefore, in a natural way, it is possible to understand the importance of investment in the purchase and use of appropriate safety equipment adapted to the working conditions in question.

However, to choose the best safety shoe, it is necessary to determine the best floor-shoe combination that translates into a higher coefficient of friction. This is where the interest in having a machine that allows testing different floors with different shoes comes in, to evaluate the coefficient friction for each case and understand if the shoe meets the safety standards.

The motivation behind this project comes from the ambition to design a machine that is able to meet the requirements of DIN 51130:2014-02 and at the same time is more affordable than the market standard. Another aspect that could be improved is the possibility of making the solution more compact, especially in terms of height, so that the application is not so restricted in terms of available space.

1.2 Goals

Given the scope of this dissertation, the goals of this article are:

- To present the existing devices for the evaluation of the coefficient of friction;
- To design an equipment to measure the coefficient of friction based on the DIN 51130 standard.

1.3 Methodology

In the first phase, the development of this dissertation was focused on the study and gaining of knowledge about coefficient of friction and safety shoes. Based on this, the study of friction between the sole of safety shoes and the floor was deepened in order to understand this phenomenon and the impact it has on workplace safety and accident prevention.

In a second phase, as the main purpose of this project is the development of an equipment to evaluate the friction in safety shoes, the mechanisms already existing in the market were investigated, followed by an in-depth study of their characteristics and requirements, focusing on the system that is the subject of standard DIN 51130.

The project of the machine was carried out based on the obtained information. To do so, the necessary calculations for the dimensioning of its components and structure were performed. Additionally, the software ANSYS was used to verify the structural integrity of the final design.

Finally, a 3D model of the project was created using SolidWorks while simultaneously dimensioning the components.

1.4 Structure of the Dissertation

This dissertation is divided into the following chapters:

In Chapter 1, a brief description of the dissertation topic is made. In addition, the main goals and the methodology adopted in its development are shown.

Chapter 2 aims to review the main equipment for the evaluation of friction on floor surfaces, as well as to known their operation and features, with special emphasis on the mechanism on which this dissertation is based. This chapter also introduces some key concepts such as friction and the gait cycle to ensure a thorough understanding of this project.

Chapter 3 explains the entire mechanical design, from the choice and dimensioning of its constituent elements, highlighting the implemented lifting system, to its structural verification using ANSYS. Additionally, it covers the preliminary calculations made to determine the loads that the system is subjected to, models that were considered for the project before the decision was made, and a three-dimensional model of the machine in the starting and final positions for various viewpoints.

Lastly, in Chapter 4, the conclusions drawn from the work developed are presented, as well as possible future work.

Chapter 2

State of the Art

This chapter examines the approaches used in the literature to link shoe friction to the danger of slipping and falling. It also examines the under-shoe dynamic circumstances during walking, as well as human gait factors that are related to slippage and their effects on the likelihood of slips and falls.

Furthermore, some of the most commonly used coefficient of friction measuring equipment are presented and reviewed.

2.1 Understanding the Gait Cycle

To better understand, slips and falls it is important to know the phases and forces that are involved during walking.

The gait cycle is divided into stance and swing phases as shown in Figure 2.1. The stance phase, which is the most important one, accounts for approximately 60% of the entire cycle and is separated into heel strike (A), loading reaction, mid-stance (B), terminal stance (C), and pre-swing (D) [7, 8]. Figure 2.2 depicts the evolution of the normal and horizontal forces during this phase.

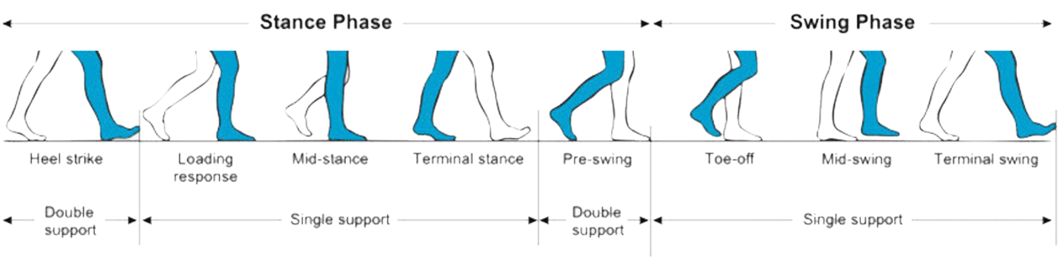

Figure 2.1: Gait Cycle adapted from [8]

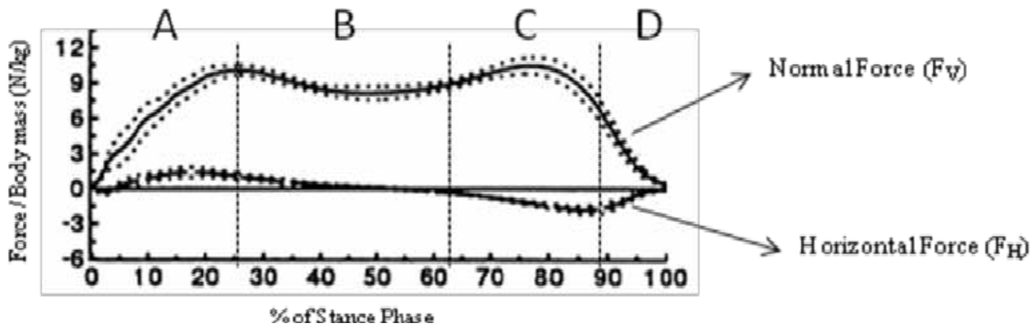

Figure 2.2: Typical ground reaction forces: Normal force (solid line); Horizontal force, (dashed line); standard deviations (dotted lines) [7]

The key times in a step are when the horizontal force reaches its peak, meaning when the demand for friction is greatest. This happens throughout the heel strike phase and the terminal stance, as shown in Figure 2.2 [7, 9]. When comparing these two stages, the initial heel impact (heel strike) is regarded as the stage with the greatest risk of falling since a person is less capable to regain balance at this moment [7].

The lack of sufficient friction between the shoe and the surface is one of the fundamental factors that lead to a slip, and it is on this that the following section's study is based.

2.2 Friction

Slip risk is measured in shoe studies using the coefficient of friction (COF) at the shoe-floor interface. The ratio of shear forces parallel to the surface to normal forces perpendicular to the surface is used to determine this value. This coefficient is difficult to calculate because it is influenced by the shoe material, the surface, shoe thread, and the contaminant [10].

A slip occurs when the available coefficient of friction (ACOF) is less than the required coefficient of friction (RCOF) [11, 10, 6] between the shoe and the surface. These two parameters are used to calculate the likelihood of slipping.

The required COF is impacted by gait biomechanics [12], and it is often measured on dry surfaces with a force plate, with human subjects walking on the floor with complete confidence and no fear of slipping [12, 13]. This is significant since it affects how the individual walks and can lead to incorrect results [14]. Thus, when a human mistakenly goes onto a contaminated surface from a dry surface, this criterion of comparing the needed and accessible COF might be used. A friction assessment tool is designed to mimic a slip when measured on flooring both with and without contaminants in order to evaluate the highest COF that may be supported at the shoe-floor contact for the ACOF.

Even though individuals are less prone to slip on dry surfaces, the devices are nevertheless designed to monitor the breakaway force, which is defined as the greatest COF that can be [13]. Knowing these values, slips can be minimized by increasing ACOF or decreasing RCOF [12].

2.3 Coefficient of Friction Measurement Equipment

The coefficient of friction can be measured using a variety of instruments. These are divided into two categories: those that measure the static coefficient of friction and those that measure the kinetic coefficient of friction.

Studies like [1, 15] show that the majority of foot slips occur during kinetic foot movement conditions, hence the kinetic coefficient of friction (KCOF) is a better indicator of the floor-contaminant-footwear friction capabilities. As a result, only kinetic friction measuring equipment will be discussed.

Within this category, there are systems that simulate human slippage circumstances, such as the pendulum, STM 603, ramp tests, and systems that do not, such as the Tortus and the SlipAlert. Other tests fall into these two categories, however, they will not be addressed since they are not preferred to the ones listed above.

The testing should preferably meet the following parameters to be as near to a human slip as possible:

- For whole-shoe devices, the normal force build-up rate should be at least 10 kN/s;
- A standard contact pressure of 200 to 1000 kPa is recommended;
- The sliding speed should range from 0 to 1.0 m/s;
- The maximum contact time before and during the COF calculation should be 600 ms [11].

It is crucial to highlight, however, that no machine can be used as an absolute reference for determining slip resistance. Certain devices may perform better than others under specific circumstances. For instance, a certain device might be effective at forecasting slips and falls on greasy surfaces but useless in wet conditions [6, 1, 16]. That is why it has to be chosen based on the nature of the conditions being evaluated.

2.3.1 Pendulum

The Portable Skid Resistance Tester, also known as the British pendulum tester, was initially designed in the 1940s to measure the slip resistance of floors in government facilities. The instrument was adopted and refined in the late 1950s to investigate problems associated with highway design and upkeep and to evaluate the frictional resistance of new roadways, railway infrastructure, and road markings [7].

Today, the pendulum is most commonly used to test the shear strength of roads, office surfaces, footbridges, shopping center floors, factories, airports, and sports facilities - both during the design and post-installation stages and in accident investigations [17].

This device measures the dynamic coefficient of friction of a floor surface. Consists of a pendulum arm with a rectangular spring-loaded rubber slider with a specified hardness that sweeps a certain area of flooring (see Figure 2.3).

This test measures the energy lost as the slider is dragged and decelerated over the surface to be tested, which influences the swing of the pendulum. This test accurately replicates the interaction between the foot heel and the floor during normal walking gait [3]. The higher the friction, the less the pendulum oscillates and the greater the value of the sliding resistance [18, 3].

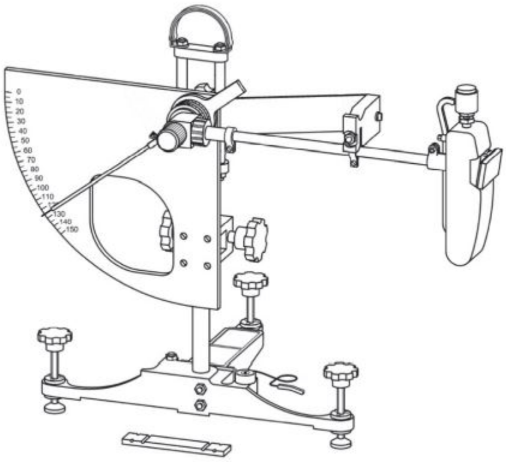

Figure 2.3: Schematic drawing of the pendulum test device [19]

The British pendulum is the only portable slip resistance meter that HSE has adopted for determining how slippery a floor is under wet and dirty circumstances. However, it must be utilised and evaluated by a skilled and knowledgeable operator in order for it to be a reliable test [18, 3].

The values measured in the tests are obtained in British Pendulum Number (BPN), which directly represent the risk of slipping, as shown in Table 2.1, and indirectly represents the friction obtained between the shoe and the floor. Although the dynamic effects of the slider's spring-loaded configuration cause a slight but noticeable variance, BPN values are typically judged to be roughly equivalent to COF times 100. Due to this, the relationship between the values obtained in BPN and the coefficient of friction is described by Equation 2.1.

$$COF_{Pendulum} = \left(\frac{110}{BPN} - \frac{1}{3}\right)^{-1} [7] \tag{2.1}$$

Table 2.1: Slip potential classification, based on British Pendulum Number (BPN) [7]

Slip Potencial	**BPN**	**COF**
High	0 - 24	0 - 0.235
Moderate	25 - 35	0.246 - 0.356
Low	36 +	0.367 +

As verified by the previous equation, the higher the BPN value, the greater the resistance offered by the surface to the passage of the rubber of the pendulum. This result is greatly influenced by the choice of rubber. The type of rubber used for this tester is determined by the analysis to be performed. That is, a hard rubber is used to simulate the use of footwear, while a soft rubber is used to simulate barefoot use such as bathroom floors,showers, and swimming pool decks [19]. For example, products tested with the moderate hardness TRL rubber will frequently be classified lower than those tested with the greater hardness “Standard Shoe Sole Simulating” rubber also known as Four S or as Slider 96 [20]. To get an idea, a 35 BPN result corresponds to a 0.36 coefficient of friction, which is usually considered as a one-in-a-million chance of slipping [21].

2.3.2 Tortus

The Tortus (see Fig. 2.4) is a drag-sled type of digital motorized tribometer that moves along the floor by dragging a rubber base.

Figure 2.4: Tortus device [22]

The tribometer records and calculates the resistance of the floor by dragging a rubber over a certain distance of at least 150 mm. The average dynamic coefficient of friction is determined after crossing the entire given distance. KCOF values greater than 0.50 indicate that the machine is having trouble dragging the rubber, resulting in a fall-resistant floor. When the KCOF value is less than 0.50, it is assumed that the Tortus moves easily and that the floor is slippery [20, 23].

In both dry and wet settings, the battery-operated instrument can be used to assess the resistance to sliding of a broad range of flooring surfaces, including ceramic tiles.

When compared to the pendulum, the Tortus has the benefit of being able to do several slip resistance tests in a short amount of time making this useful for swiftly evaluating and/or evaluating numerous regions of a vast floor to see if slip resistance changes in different areas [23]. Moreover, because it does not require any connecting wires or a computer, this device is completely portable. Nevertheless, because this test is a patented device, there is no standard to back it up, however, the Ceramic Tile Institute of America (CTIOA) has sponsored it as a secondary standard since 2001, after the pendulum [20].

2.3.3 SlipAlert

The SlipAlert type instrument tribometer slides down an aluminium ramp with a defined slope and height before contacting the ground, as shown in Figure 2.5 [23].

Once on the ground, the SlipAlert slides on two front wheels and a rubber slider at the rear (see Fig. 2.6), mounted at the same angle to the ground at the moment of impact as the Pendulum slider.

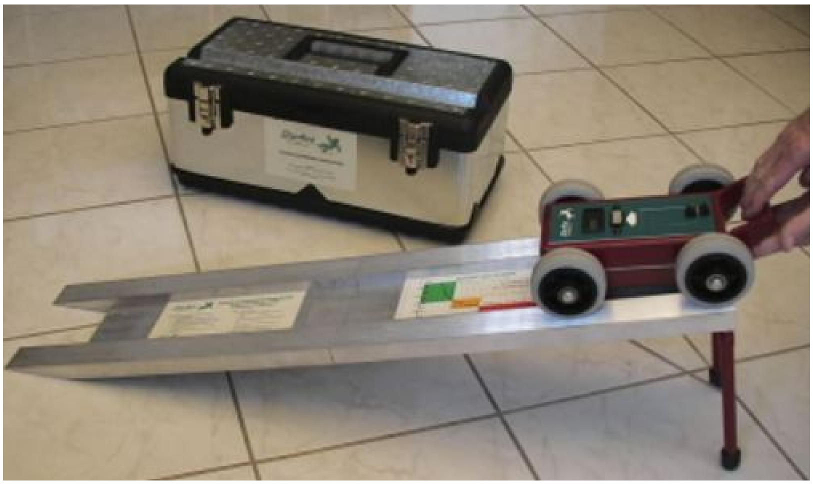

Figure 2.5: SlipAlert [22]

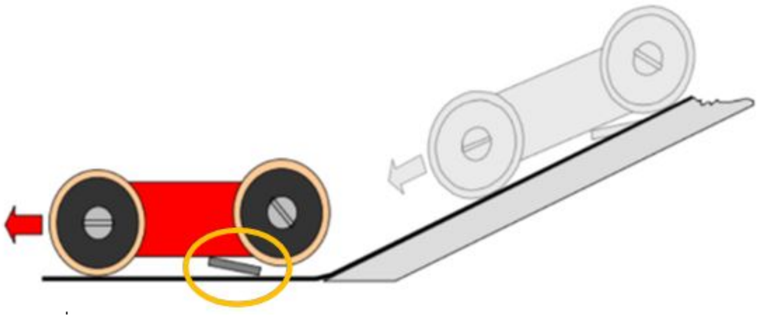

Figure 2.6: SlipAlert slider rubber detail adapted from [24]

The unit includes an integrated digital display that shows the distance traveled, which is then easily converted into a coefficient of friction using the diagram attached to the ramp [3, 23]. This chart can be seen in detail in Figure 2.7. As expected, the more slippery the ground, the less energy is absorbed and the longer the distance traveled by the SlipAlert [23].

Studies demonstrate that this mechanism can produce good results with a good correlation to the Pendulum [3, 23] as proven in Figure 2.8, being able to distinguish between dry and wet flooring. Moreover, when the COF values acquired by the two devices deviate, the SlipAlert tends to err on the side of caution by underestimating the existent slip resistance. In other words, using this test alone, it is unlikely that a pavement classified as safe is harmful [3].

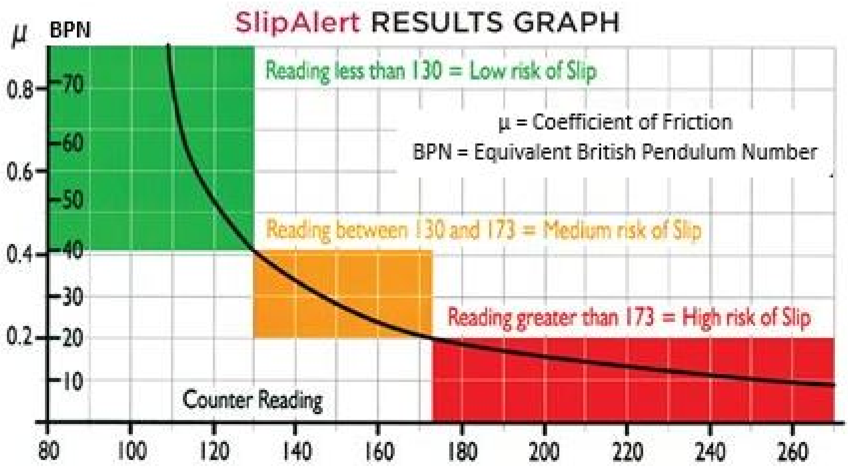

Figure 2.7: Conversion chart adapted from [25]

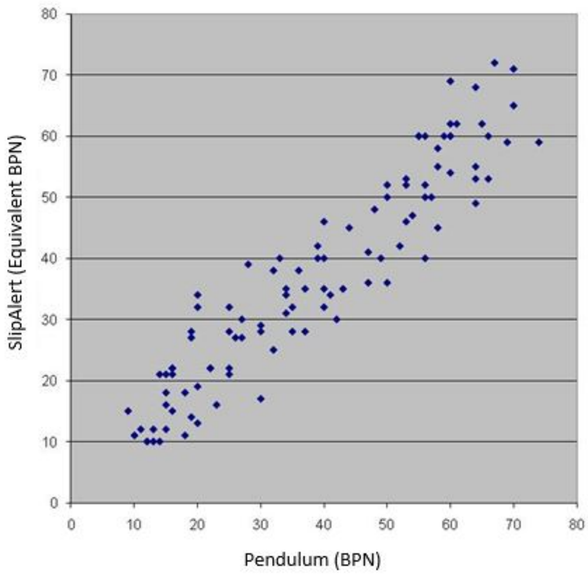

Figure 2.8: SlipAlert Correlation with BPN adapted from [25]

Although it is a lightweight and practical solution, it has some drawbacks, such as requiring a larger floor surface than the pendulum and is not suggested where friction measurements are crucial, such as in criminal investigations or product requirements [3, 23].

2.3.4 STM 603

The STM 603 Slip Resistance Tester is a computer-controlled friction tester for testing different shoe-floor-contaminant combinations that reproduces the sole dynamics during the stages where slip is most prone to occur [7, 26].

To perform the test, the shoe is fitted onto a shoemaking last and attached to the cage plate of the friction rig [26], as shown in Figure 2.9. The test surface is located underneath the shoe.

At the beginning of the test, a pneumatic cylinder lowers the cage plate, and consequently the shoe contacts the ground and applies a pre-defined vertical force. A few seconds later, a motor moves the floor and two force transducers measure the horizontal and vertical force between the two surfaces, and a ratio of these two is displayed as COF on the final graph.

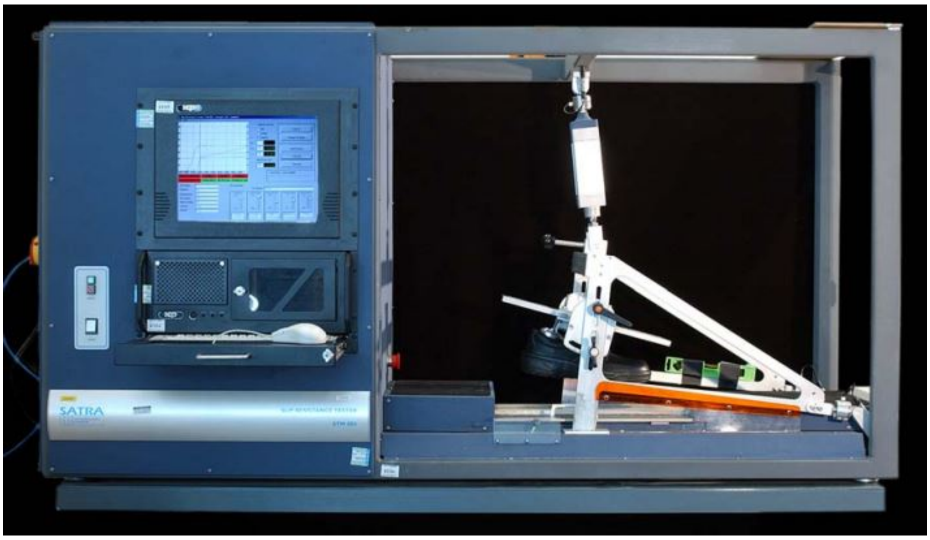

Figure 2.9: The STM 603 Slip Resistance Tester from [26]

This equipment has its own unique software which allows the test parameters to be controlled within its operating limits. These include the:

- Vertical force applied
- Slip speed: the speed at which the floor surface is moved under the footwear;
- Snapshot low: timestamp at which the horizontal force measurement begins;
- Snapshot high: timestamp where the horizontal force measurement ends;
- Static contact time: the time interval between the shoe contact with the test surface and the beginning of its movement;
- Average over: the number of COF measurements to be taken per test [26].

As stated in Chapter 2.1, the moment when half of the body weight is being supported, just after heel strike and just before toe lift, is when a slip is most likely to happen. Therefore, the most common use of this test is to recreate the instant when the heel strikes the ground, for such, the shoe is mounted so only the back of the heel contacts with the test surface and that slipping occurs in a forward direction [27]. Nevertheless, it is possible to position the shoe in other ways such as flat contact or sideways-on.

At the end of the test, a graphic like the one in Figure 2.10 is obtained with four lines representing the vertical and horizontal force, the coefficient of friction, and the distance traveled [26, 27]. Since the test is dynamic, excessive static friction cannot be used to cover up poor sliding resistance, providing more accurate findings [7].

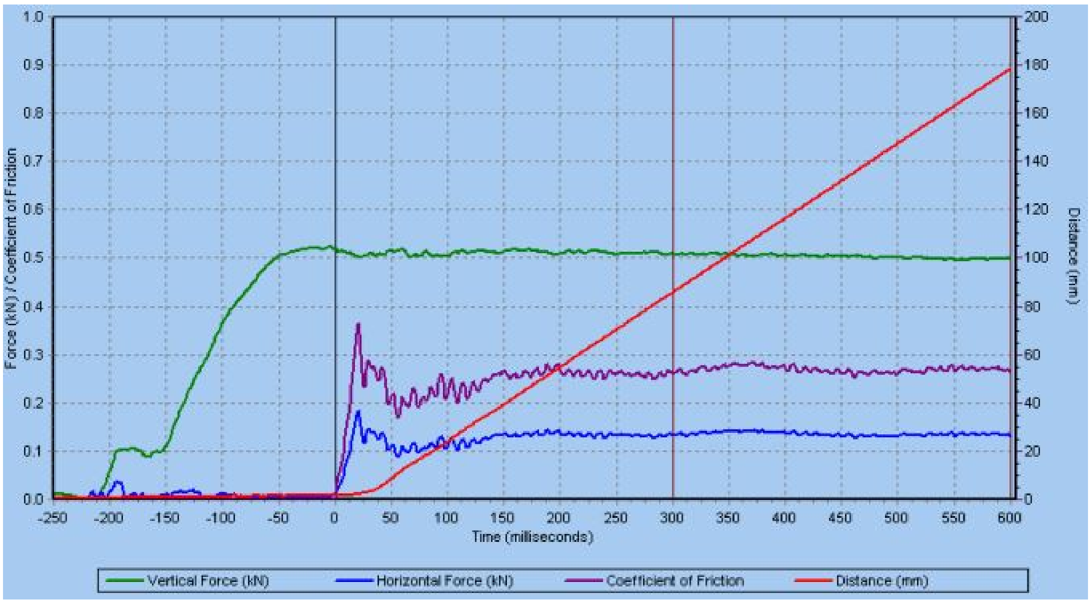

Figure 2.10: Typical plot displayed by the STM 603 [26]

2.3.5 Ramp Test

Ramp testing is a human subject-based technique that involves the use of trained test subjects walking with an upright posture in a standardized way [23] forward and backward, facing downwards, on a platform over a contaminated floor sample [9, 19, 16]. To ensure the safety of the walkers, the test apparatus is equipped with a safety harness and a fall protection system as shown in Figure 2.11 [26].

The coefficient of friction of the flooring under test can be estimated using the average angle of inclination at which the tester slips [16] and can be converted using a rating scale.

These tests are based on German standards, namely DIN 51097 and DIN 51130. The first is used to test floors used in wet areas such as swimming pools, where barefoot walking is expected. For this purpose, the test is done barefoot and soapy water is used as a contaminant [26, 19, 27, 16]. On the other hand, DIN 51130 uses heavily treaded safety shoes with soles and heels made of a certain material and pattern and engine oil as a contaminant [9, 27]. The type of shoe under study belongs to the range of personal protective equipment (PPE), which is commonly used in factories. This standard is used to evaluate flooring materials used in areas with substantial levels of oil contamination [9]. In addition to these discrepancies between standards, each one has a different floor grading scale. Tables 2.2 and 2.3 show, respectively, the DIN 51097 and DIN 51130 classes.

Table 2.2: Classification of surface according to DIN 51097 [23]

Classification	Angle [º]	Coefficient of Friction	Recommended use
A	12 - 17	0.21 - 0.31	Communal changing rooms
B	18 - 24	0.32 - 0.42	Swimming pool surrounds
C	> 24	> 0.42	Swimming pool ramps or steps leading to the water

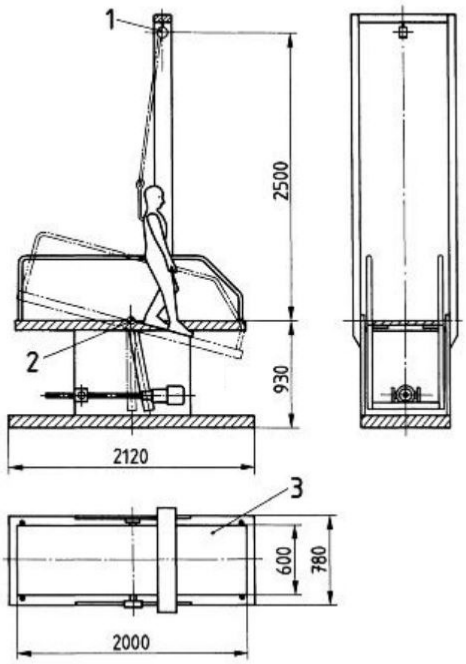

Figure 2.11: Example of a test apparatus with safety equipment: 1- Safety harness and fall protection system; 2- Angle transmitter; 3- Inclinable platform upon which the flooring test piece is attached. Adapted from DIN 51130 [28]

Table 2.3: Classification of surface according to DIN 51130 [28]

Classification	Angle [°]	Coefficient of Friction	Recommended use
R9	6 - 10	0.11 - 0.18	Dry indoor areas
R10	10 - 19	0.18 - 0.34	Indoor or outdoor areas where there may be a minimal wetting remaining
R11	19 - 27	0.34 - 0.51	Areas which may be subject to heavy wetting of the surface
R12	27 - 35	0.51 - 0.70	Wet areas
R13	> 35	> 0.70	Areas which may be subject to heavy wetting of the surface combined with other contaminants, steps or ramps

It is important to note that for a given combination of factors, i.e. floor-contaminant-shoe, the inclination angle that is obtained as the maximum inclination does not translate into any level of safety in the use of the same floor on surfaces with inclinations lower than the maximum. The fact that these tests are made based on an angle is just a means to an end for assessing the slip resistance of a surface when used flat [9].

This method of assessment can be done with different combinations of shoe types and wearing conditions of the flooring, allowing to define more precisely the safe wearing conditions of the flooring, but it does not allow *in situ* measurements since it is a laboratory test and due to its dimensions it is not portable [26, 27].

2.4 Conclusion

This section discusses some of the coefficient of friction evaluation equipment currently available. It was noted that the measurement properties and settings of currently available coefficient of friction measurement instruments differ significantly from those seen in biomechanical tests and from slips. They also provide extremely varied outcomes, although the majority of these devices can nonetheless produce useful, user-accepted data. By improving the bio-fidelity and tribo-fidelity of the equipment, their conditions and characteristics get closer to what actually happens at the shoe-floor interface during a slip, and better results can be obtained.

All these methods allow the surfaces of hospitals, factories, schools, shopping malls, and others to meet the safety standards for the minimum required coefficient of friction.

In addition, by analysing the gait cycle it was possible to understand why some equipment tries to reproduce the heel contact moment to evaluate the coefficient of friction.

Chapter 3

Mechanical Project

From the project requirements, several ideas for the machine's lifting system were developed until the final concept was reached. After determining the functional model, and defining the essential components, it was necessary to find the dimensions required for them to function according to the project specifications.

The most suitable materials were chosen, always following the advice of the suppliers, and dimensioning was done according to material resistance criteria and applicable international regulations.

In addition, the stability of the structures were tested using the software ANSYS.

3.1 Design Specifications

The DIN 51130 standard, which regulates ramp tests for friction measurement, was used as a starting point, and from there the requirements that the equipment has to meet to perform the intended tests were taken. These are as follows:

- Walkable area: 2000 x 600 [mm];
- Testing area: 1000 x 500 [mm];
- Permissible inclination: 0 to 40°;
- Maximum angular velocity: 1º/s;
- Angle of inclination must not fluctuate by more than ± 1º when walked along;
- Continuous lifting movement or in 0.5º increments;
- Handrails to ensure the safety of the tester;
- Safety harness and fall protection system [28].

3.2 Design Ideas

During the mechanical design phase, the first two major decisions that had to be made were regarding the rotation point of the system and the mechanism responsible for raising or lowering the platform.

The following ideas emerged in response to these two questions until the final solution was reached, after which the necessary calculations and tests were performed to complete the project. It should be noted that preliminary calculations were performed for each of the models considered to determine the load capacity required in each case.

3.2.1 Preliminary Designs

From the very beginning, contrary to what is currently available on the market, an attempt was made to create a complete mechanical solution.

A vertically mounted S-model screw jack (translating screw) that lifted the platform was the first model considered. The platform's axis of rotation was located at the far end. This idea was quickly abandoned due to several issues, including the need for a very large stroke, which would be impractical for the required lifting force; because it is impossible to lift completely vertically due to platform rotation, the screw jack would have to be able to slightly rotate, which would also create instability. Furthermore, due to the model of the screw jack that would have to be used, a very large space underneath the platform would be required to accommodate it, resulting in a machine with a height of approximately 3 m when fully raised. In addition, the height of the tester would limit where the machine could be used.

A modification of this model was to consider rotating in the middle and lifting at the end with the same mechanism, but this also required a high stroke and the final height of the equipment would also be very high.

A third approach was to place the S-model screw jack horizontally, pushing a perpendicular bar, connected to two bars attached to the upper platform. However, in this case, the force tends toward infinity in the beginning of the movement. One way around this problem was to apply the screw jack directly by pushing/pulling a diagonal bar that would be sliding on wheels, but the force that would have to be applied would also be too high due to the screw jack's travel restrictions.

Another impediment to this solution would be the space required to accommodate the screw jack as it rotated to achieve the full range of motion.

Another option was to use a horizontal R-type (rotating screw jack), with the advancing component attached to a bar connected to the moving platform. This solution introduces two issues: bending of the screw, because this equipment is only designed to accommodate forces in the direction of its movement, and here it would be subjected to forces perpendicular to its movement, and depending on the length of the connecting bar, the screw jack would have to have a high rotation, resulting in a very tall machine.

Finally, the course was completely altered, and a seesaw solution was considered, in which a gear powered by a motor rotated and engaged with a timing belt, causing the top to descend. The issue here is that even using a chain tensioner would be an extremely unstable solution that would not be appropriate due to system requirements such as varying the elevation angle when the person walks. Furthermore, this would give the tester a sense of insecurity.

In all of these models, an electro-hydraulic cylinder has been proposed to replace the screw jack, but the available strokes are insufficient. To be used in smaller strokes, their load capacity would have to be much higher than it is now.

Below is an overview in the tabular form of the models and the reasons why they do not work (see Table 3.1).

Table 3.1: Overview of the early designs

Models	Mechanism	Position	Rotating Point	Problems
1	Screw jack - Type S	Vertical	Left	- Rotation - Space - Stroke
2	Screw jack - Type S	Vertical	Middle	- Rotation - Space - Stroke
3	Screw jack - Type S	Horizontal	Left	- Infinite force - Space
4	Screw jack - Type S	Diagonal	Left	- Load capacity - Stroke
5	Screw jack - Type R	Horizontal	Left	- Buckling - Space
6	Gear	—-	Middle	- Instability
7	Electro-hydraulic cylinder	Diagonal/Horizontal/Vertical	Left/Middle	- Stroke - Load capacity

3.2.2 Final Design

After several attempts involving a mechanical system, it was decided to lift the platform using a hydraulic cylinder. Using a pneumatic cylinder was never considered because it is sensitive to vibrations, which would be common due to a person walking on the platform, and lacks precision, which would possibly necessitate adding more equipment to the pneumatic system to make it work at the desired levels.

It was eventually decided on a rotation of the platform at the end performed by a hydraulic cylinder that is mounted underneath the platform. This solution ensures structure stability during operation, does not result in very high equipment when fully raised, and a good balance between required force and required stroke.

Even though less force would be required, performing the rotation halfway along the length of the platform was not chosen because it would result in a less compact unit with a higher final height.

A schematic of the chosen system is shown in Figure 3.1.

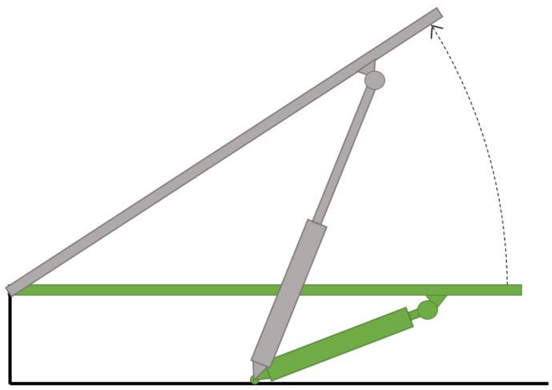

Figure 3.1: Schematic of the final configuration of the lifting system. Components in green are in the starting position and in gray in the final position.

3.3 Three-dimensional Project

A 3D modeling was performed in SolidWorks 2021 of the entire project to ensure the correct dimensions of all components, to certify that there are no geometric interferences between them and to facilitate the modeling process in ANSYS 2022. In addition, a three-dimensional visualization allows a better perception of the final design.

3.3.1 Initial Position

For initial platform position different views of the machine are presented. In Figure 3.2, it is possible to see the isometric view of the machine with a figure that has 1.75 m as scale reference. Figures 3.3, 3.4, 3.5 and 3.6 show the front, side, top and bottom views, respectively.

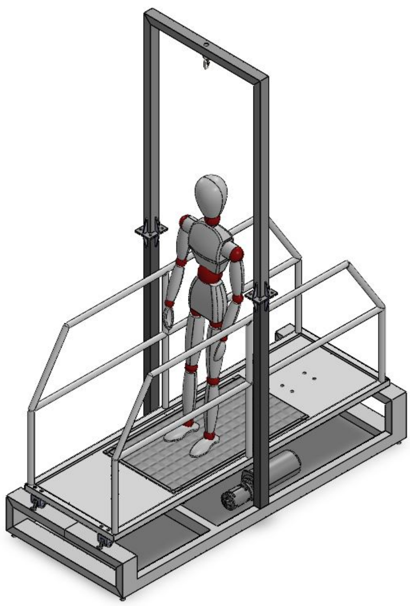

Figure 3.2: Isometric view of the machine with a scale model

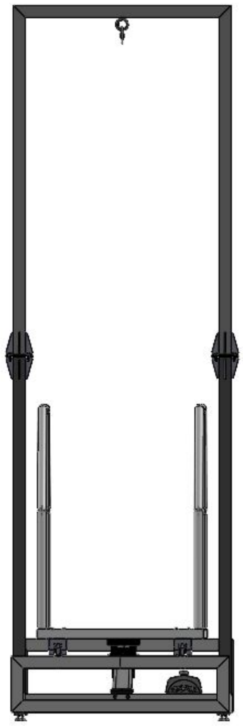

Figure 3.3: Front view of the machine

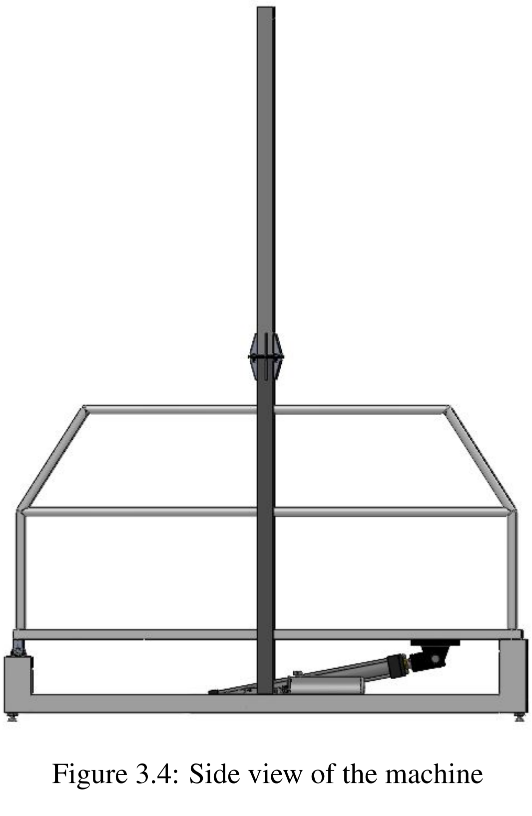

Figure 3.4: Side view of the machine

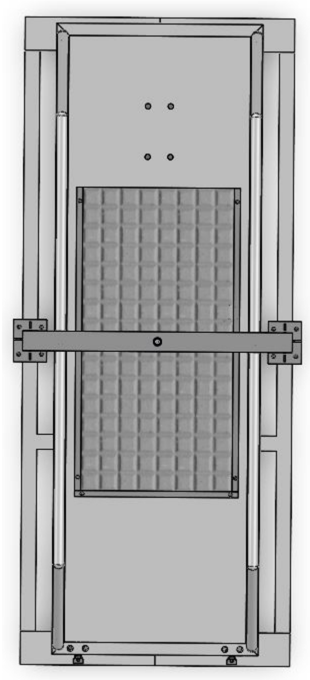

Figure 3.5: Top view of the machine

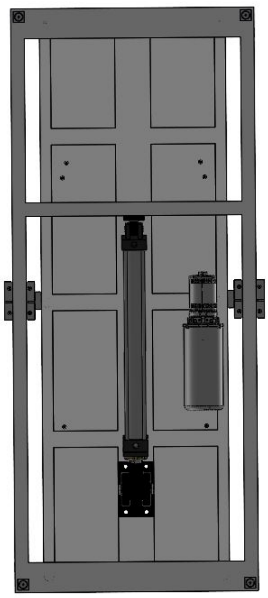

Figure 3.6: Bottom view of the machine

3.3.2 Final Position

For initial platform position different views of the machine are presented. In Figure 3.7, it is possible to see the isometric view of the machine. Figures 3.8 and 3.9 show the front and the side views, respectively.

Figure 3.7: Isometric view of the machine

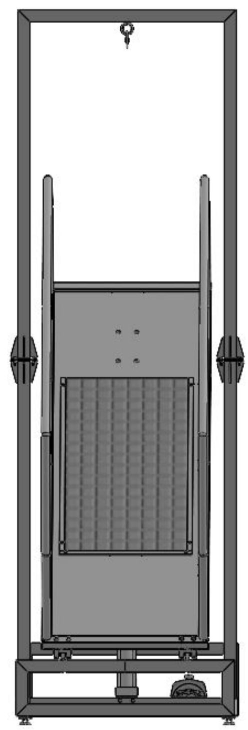

Figure 3.8: Front view of the machine when fully raised

Figure 3.9: Side view of the machine when fully raised

In Appendix A are shown 2D drawings of the final structure in the initial and final position with the main dimensions represented to give a better perspective of the space occupied by the machine.

3.3.3 Rotation System

The system that allows the rotation of the platform can be seen in Figure 3.10 and is composed of the U-shaped part (fork), pillow block unit, shaft and the associated fastening screw. This set is used twice in the final equipment.

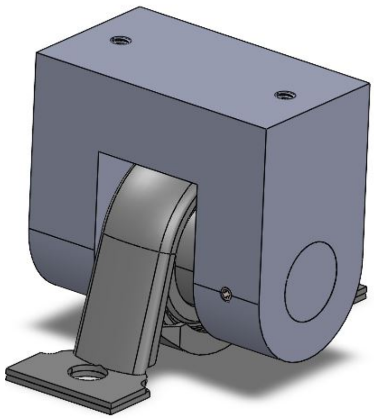

Figure 3.10: 3D of the rotation system

3.4 Choice of Materials for the Different Components

This chapter discusses the materials to be used in the main components, taking into account not only the mechanical requirements but also the surrounding conditions of their use, in the sense of not only resisting the efforts imposed in the worst possible conditions but also their durability to wear and degradation, guided by the idea of building something durable that requires little maintenance to operate safely.

3.4.1 Main Body

During the design phase, it was decided that the main body of the machine, which consists of the platform, base, and safety harness support, would be made of steel and welded together. On this basis, AISI 1024 steel was chosen, which is unalloyed construction steel with a wide range of applications, primarily in welded construction [29].

This material was chosen over stainless steel because the latter would not only be more expensive but would also make welding the components more difficult, increasing the overall cost of the machine.

However, since the machine is in contact with oil due to the kind of tests that are performed on it, a solution to the oxidation problem had to be found. The simplest method discovered was to paint the various components with an anti-corrosive paint after they had been assembled, thereby creating a protective layer.

The main properties are shown in Table 3.2. For more information about the material see Appendix B.1.

Table 3.2: AISI 1024 steel mechanical properties [29]

	Density [g/cm^3]	Yield Strength [MPa]	Tensile Strength [MPa]
AISI 1024	7.80	355	470 – 630

3.4.2 Shafts

For the shafts it was chosen the AISI 1045 steel, which corresponds to a medium carbon construction steel that can be used as is or heat treated. It is a steel with a wide range of applications, appearing in almost all families of the metal-mechanical sector [30].

The main properties are shown in Table 3.3. For more information about the material see appendix B.2.

Table 3.3: AISI 1045 steel mechanical properties [30]

	Density [g/cm^3]	Yield Strength [MPa]	Tensile Strength [MPa]
AISI 1045	7.84	330 - 640	580 - 770

3.4.3 Other Components

Components such as the shafts, the bushings that guide the fork fixing bolts and those that guide the pillow block unit fixing bolts, and the bars that allow the floor to be tested and fixed will all be made of the same material as the main body, AISI 1024.

3.5 Load Analysis

The initial part of the mechanical project entails drawing a free body diagram (see Figures 3.11 and 3.12) to determine the ideal combination of angles and lengths for the hydraulic cylinder's load capacity and needed stroke.

To be safe, it was estimated that the tester had a mass of 200 kg (F_t), the platform had a mass of 250 kg (F_p), and the acceleration of gravity was 10 m/s^2. Furthermore, because the worst-case scenario should always be considered, the tester was assumed to be at the far end of the support. Figure 3.13 shows the forces applied on the system when it is in the initial position.

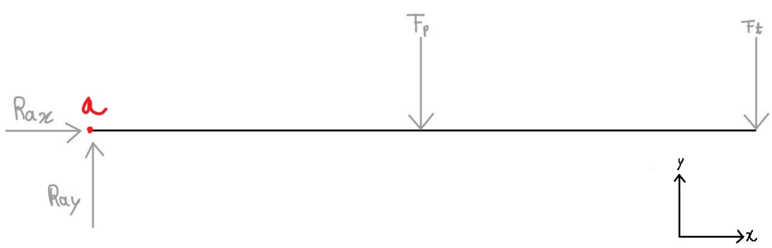

Figure 3.11: Free-body diagram of the platform in the starting position

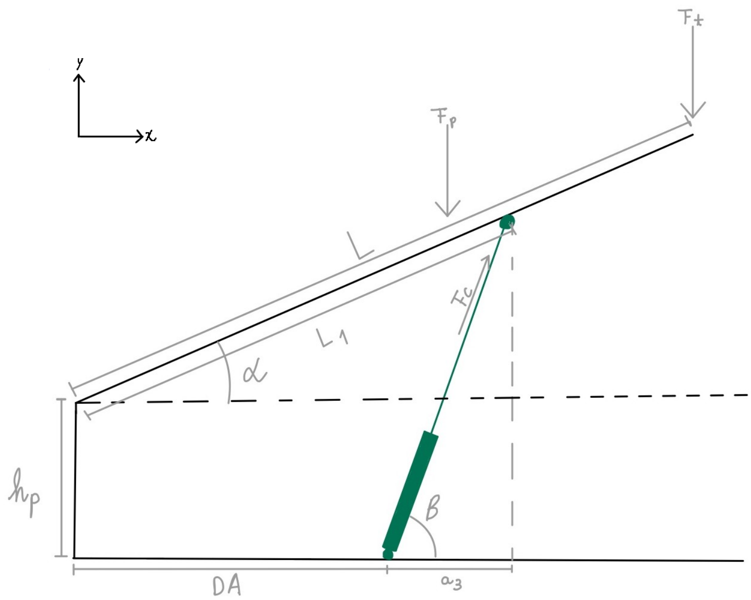

Figure 3.12: Diagram of the machine in the upper position

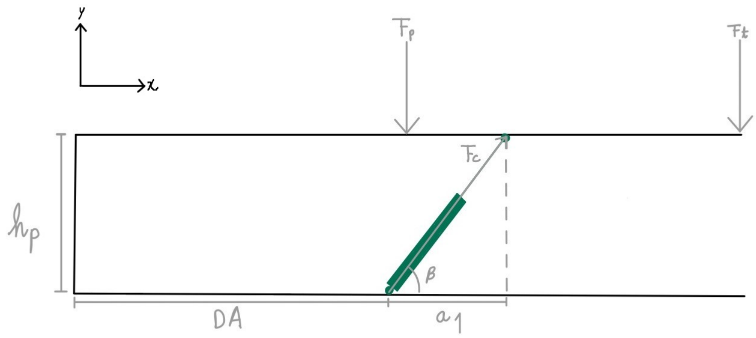

Figure 3.13: Diagram of the machine in the starting position

The Equations that results from the free-body diagram are as follows:

$$\sum F_x = 0 \Rightarrow R_{ax} + F_c \cos\beta = 0 \tag{3.1}$$

$$\sum F_y = 0 \Rightarrow R_{ay} + F_c \sin\beta = F_t + F_p \tag{3.2}$$

$$\sum M_a = 0 \Rightarrow F_t \times L \times \cos\alpha + F_p \times \frac{L}{2} \times \cos\alpha = F_c \times (L_1 \times \cos\beta \times \sin\alpha + L_1 \times \sin\beta \times \cos\alpha) \tag{3.3}$$

$$a_1 = \frac{h_p}{\tan\beta_{initial}} \tag{3.4}$$

$$DA = L_1 - a_1 \tag{3.5}$$

$$a_2 = L_1 \times \cos\alpha_{final} \tag{3.6}$$

$$a_3 = a_2 - DA \tag{3.7}$$

$$L_{cfinal} = \frac{a_3}{\cos\beta_{final}} \tag{3.8}$$

$$Stroke = L_{cfinal} - L_{cinitial} \tag{3.9}$$

Where:

F_c: Hydraulic cylinder force [N];

R_{ax}: Reaction on the x-axis at the support [N];

R_{ay}: Reaction on the y-axis at the support [N];

F_p: Platform weight force [N];

F_t: Tester weight force [N];

α: Platform elevation angle [º];

β: Angle that the hydraulic cylinder makes with the x-axis [º];

L: Platform length [mm];

h_p: Distance, vertically, from the floor to the support [mm];

L_1: Distance between cylinder and platform contact and support [mm];

DA: Horizontal distance between cylinder and support [mm];

$L_{cinitial}$: Hydraulic cylinder length in the initial position [mm];

L_{cfinal}: Hydraulic cylinder length in the final position [mm];

Stroke: Hydraulic cylinder stroke [mm].

The trigonometric relation that relates the $\beta_{initial}$ to h, L_1, and a_1 is given by Equation 3.10 and β_{final} is given by Equation 3.11 where α = 45º.

$$\beta_{initial} = \tan^{-1}(\frac{h}{a_1}) \tag{3.10}$$

$$\beta_{final} = \tan^{-1}(\frac{h_p + L_1 \times \sin\alpha}{a_1}) \tag{3.11}$$

Due to the large number of variables, h and $L_{cinitial}$ were varied until an optimal combination was obtained. The cylinder force and the reactions for various values of L_1 were then calculated.

It was decided for an L = 2080 mm because the minimum length of the walking area is 2000 mm according to the standard and for a h = 400 mm to ensure enough space for the hydraulic cylinder without the platform being too high above the floor level. The cylinder length $L_{cinitial}$ was obtained according to the stroke that was entered in the supplier's online cylinder configurator. As a result, the actual value of the stroke and the cylinder force for the different lengths of L_1 were changed until a favorable combination of values was reached. This decision was made in an effort to strike a balance between a cylinder force that was reasonably low and a cylinder stroke that wasn't excessively high. The length of the cylinder was determined to be 885 mm when fully retracted. Table 3.4 displays the values obtained for the cylinder force and support reactions for these dimensions.

Table 3.4: Force of the hydraulic cylinder and support reactions for the different L_1 distances

L_1 [mm]	Initial α = 0º						Final α = 45º				Stroke [mm]
	F_c [N]	R_{ax} [N]	R_{ay} [N]	β [º]	a_1 [mm]	DA [mm]	β[º]	a_2 [mm]	a_3 [mm]	L_c [mm]	
1220	12 259.43	-10 935.77	-1 040.98	26.87	789.45	430.55	71.11	862.67	432.12	1 334.56	449.56
1380	10 838.04	-9 667.85	-398.55	26.87	789.45	590.55	74.36	975.81	385.25	1 428.73	543.73
1450	10 314.83	-9 201.13	-162.07	26.87	789.45	660.55	75.65	1 025.30	364.75	1 471.24	586.24
1500	9 971.00	-8 894.43	-6.67	26.87	789.45	710.55	76.52	1 060.66	350.11	1 502.03	617.03
1600	9 347.81	-8 338.52	275.00	26.87	789.45	810.55	78.17	1 131.37	320.82	1 564.62	679.62
1700	8 797.94	-7 848.02	523.53	26.87	789.45	910.55	79.69	1 202.08	291.53	1 628.39	743.39
1800	8 309.17	-7 412.02	744.44	26.87	789.45	1 010.55	81.09	1 272.79	262.24	1 693.22	808.22
1900	7 871.84	-7 021.91	942.11	26.87	789.45	1 110.55	82.39	1 343.50	232.95	1 759.00	874.00
2080	7 190.63	-6 414.25	1 250.00	26.87	789.45	1 290.55	84.50	1 470.78	180.23	1 879.44	994.44

The critical moment is at the beginning of the movement when the platform is parallel to the ground, so the value of the cylinder force was only calculated for that instant.

After analysing the results, the option with the cylinder applied 1500 mm (L_1) from the support was chosen, resulting in a required force of 9971.00 N and a stroke of 617.03 mm.

With this in mind, the next step was to design the components.

3.6 Dimensioning of the Components

3.6.1 Platform

The Platform (see Fig. 3.14) is composed of three elements: a metal plate 2000 x 600 x 3 mm, a frame consisting of a square profile with 40 mm side length and 3 mm in thickness (see Fig. 3.15), and a support structure (see Fig. 3.15) which is welded together using rectangular profiles of 60 x 30 mm with a thickness of 3 mm and of 100 x 30 x 3 mm. Intermittent welding is used to join these three components.

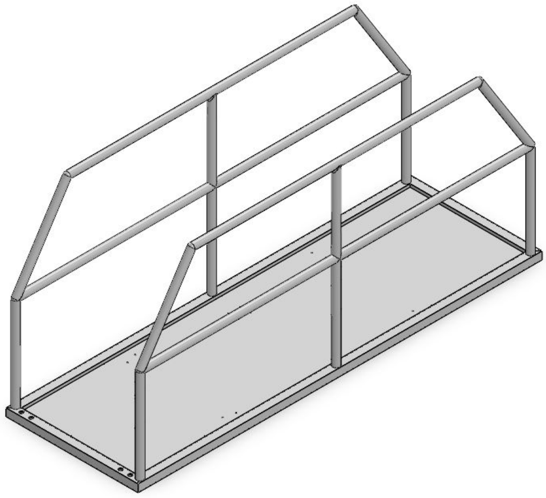

Figure 3.14: 3D design of the platform

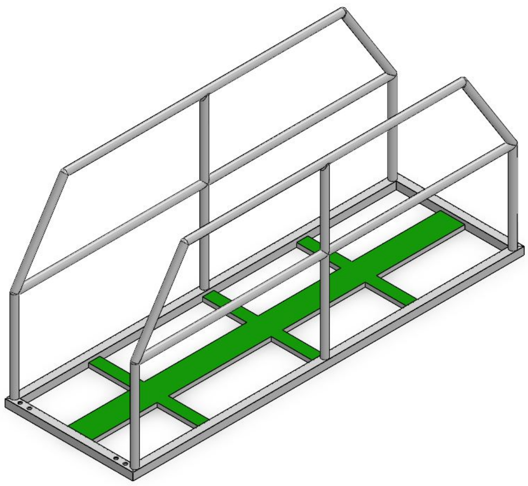

Figure 3.15: 3D design of the frame (grey) and the support structure (green)

The supporting structure was designed with a grid-like appearance rather than a cross to allow the cylinder to be fixed and to facilitate the welding of the components. Furthermore, this enables better and stronger hydraulic cylinder mounting.

3.6.2 Base

For the base it was chosen a welded construction of two types of profiles. At the ends rectangular profiles of 110 x 50 mm with 5 mm thickness were used and in the connections between the ends 75 x 50 x 3 mm profiles were used, and for the intermediate connection, which supports the hydraulic cylinder while providing more stability, a square profile of 50 mm on a side with 5 mm thickness was chosen.

The dimensions of this structure were determined based on the components that were going to be attached to it such as the pillow block units, the cylinder and the harness support. Figure 3.16 shows the 3D drawing of the base.

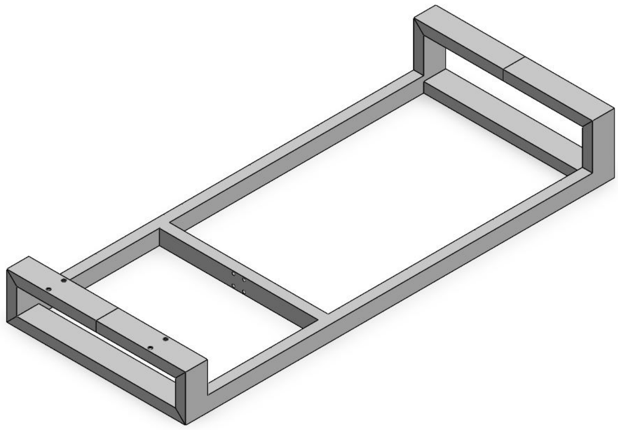

Figure 3.16: 3D design of the base

3.6.3 Safety Harness Support

One of the requirements listed in Chapter 3.1 is that there must be a safety harness to ensure the safety of the tester when slipping and possibly falling. In light of this, there were two possible solutions: either design a support structure and harness mounting with assembly on the remaining parts of the machine or do nothing and mandate that the machine could only be installed and tested in a position where a harness could be attached.

Analysing these hypotheses, it was decided to make a more complete machine, creating a support structure, so that its use would not be so restricted by the machine's place of application. As a result, a U-shaped structure was created (see Figure 3.17), which is made of two bars that are welded to the base and the upper, also U-shaped, component. To make the system easier to transport,if needed, it was chosen to build in this manner rather than create a whole structure welded to the base. For this support, rectangular profiles of 75 x 50 x 5 mm were used.

To connect the two components, plates were created to weld the components together and then assemble them using M6 screws, washers, and nuts. To maintain symmetry and a favorable distribution of forces, four screws were placed in each connection as shown in Figure 3.18. In addition, to reinforce the connection between the connecting plate and the component, ribs were welded on each side of the part. These are chamfered to avoid sharp edges and to prevent handling accidents and also to prevent stress concentration at the common point between the connection of the three pieces.

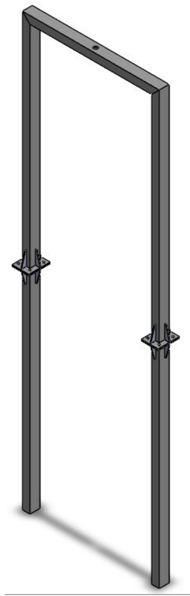

Figure 3.17: 3D model of the safety harness support structure

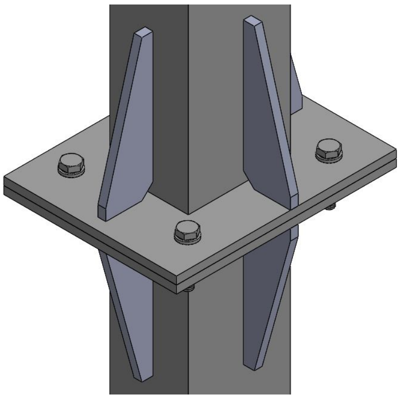

Figure 3.18: 3D model of the connection of the bars to the U-shaped structure

From the geometric simplification made of the U-shaped component, represented in Figure 3.19, it is possible to calculate the force required for each screw.

Assuming a force of 2000 N when the tester falls, it can be stated that each support R_{ey} and R_{dy} has to bear a load of 1000 N. This dividing by the 4 bolts gives 250 N for each. For an 8.8 screw class, these have a tensile strength of 800 MPa/mm^2 and a yield strength of 640 MPa/mm^2, and assuming an M6 screw that has a resistant section area of 18,99 mm^2, maximum core stress of 13.16 MPa is obtained, a very low value relative to the maximum that it can withstand. Therefore, the type of screw used was ISO 4014 hex-head screw - M6x30 - 8.8.

A smaller screw could have been used but it was considered that this one presented a good compromise between length, force that it holds, and the feeling of security that it transmits due to its size.

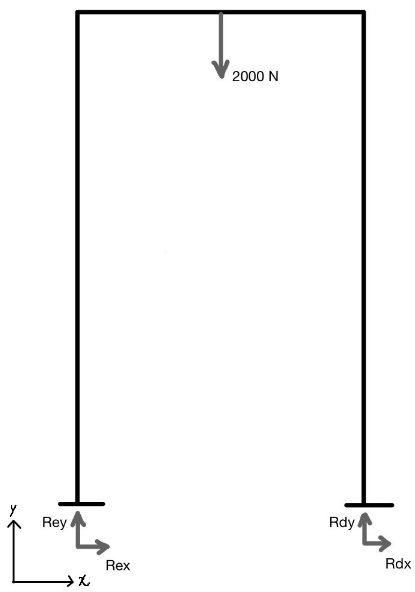

Figure 3.19: Free-body diagram of the upper part of the safety harness holder

Since it is necessary to secure the harness, a hole was drilled centered at the top of the harness support structure and a small cylinder with a 21 mm deep tapped hole was welded to it. Note that, as with the bushings, the cylinder has chamfers as well as the hole so that there is a small area all around free for welding rather than on top of the surface. This makes the final finish better while ensuring a better weld. This cylinder allows the eyelet to be screwed onto which is mounted a carabiner where the harness rope will be fixed.

As for the carabiner, one was chosen that guaranteed that it could withstand a load of more than 250 kg, to account for the force that the tester makes when falling and with its weight, with a safety margin. The model chosen was the JSP FAR0902 from RS Components which holds 23 kN and closes with a locking nut so it guarantees extra safety [31]. To check its dimensions and characteristics see Appendix C.1.

For the eyebolt, the stress in the thread core was calculated by Equation 3.12 to verify the ideal thread diameter. It turned out that for an M12 and a thread length of 20.5 mm, the core stress is 31.169 MPa, which is much lower than the 450 MPa yield strength of the material, ensuring that the thread can withstand the forces it is subjected to.

$$\sigma_c = \frac{4 \times F_a}{\pi \times d_i^2} \tag{3.12}$$

Where:

σ_c: Core stress [MPa];

F_a: Applied force [N];

d_i: Smallest thread diameter [mm].

Furthermore, according to the supplier (see Appendix C.2), an M12 eyebolt can withstand a vertical force of 3.4 kN and a 45° force of 2.4 kN, proving once again that the eyebolt and rope are capable of holding the tester in a possible fall. More information about the chosen eyebolt can be seen in the previously mentioned Appendix.

The form of assembly of these two objects can be seen in Figure 3.20.

Figure 3.20: 3D model of the eyelet and carabiner assembly

3.6.4 Hydraulic Cylinder

When dimensioning the cylinder, it is necessary to take into account several details regarding the cylinder mounting, working pressure, and stroke. Using Parker's catalog [32], this process can be carefully carried out.

The minimum force that the cylinder must guarantee, as stated in Chapter 3.5, is 9971.00 N. To be on the safe side, a safety coefficient of 1.5 is assumed, and $F_c \geq 14956.50$ N is used.

First, the HMI series of hydraulic cylinders was chosen based on the manufacturer's recommendation for the intended application. Then, among the existing mounting styles (see Appendix D.1), pivot mountings (Styles B, BB, SB) were chosen because they should be used where the machine member to be moved travels in a curved path, as in the case of the platform. The BB style was selected from among these options since it is recommended when the curved path of the piston rod travel is in a single plane.

According to the catalog, this mounting style has a stroke factor of 2, but that is for cases where the cylinder is pivoted and rigidly guided, which is not the case here, so a stroke factor of 3 was preferred (see Appendix D.2), which is for cases where the hydraulic cylinder is pivoted and supported but not rigidly guided [32]. The basic length of 1851.09 mm is obtained by multiplying this factor by the required stroke (620 mm). With this information, it is possible to examine Figure 3.21 and confirm that the indicated piston rod diameter is 45 mm and that a stop tube with a length of 50 mm is required. This means that the gross stroke is 670 mm, which is the sum of the stroke and the stop tube length.

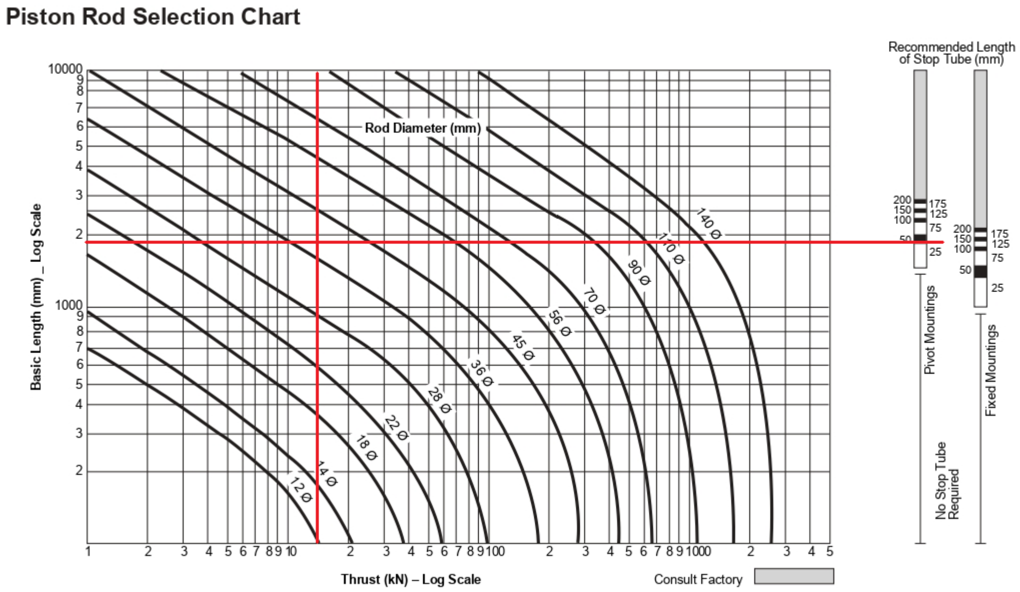

Figure 3.21: Piston rod selection chart [32]

To choose the optimum bore diameter, the resulting push and pull force must be checked against the operating pressure. The numbers inside the red line in Figure 3.22 correspond to those that ensure the required force to lift the platform although some of these are not considered due to a smaller than necessary bore diameter. As for the pull force, using Figure 3.24, it is possible to determine its value by subtracting the reduction that occurs when pulling. The values obtained are shown in Table 3.5 and the possible values for the pull force are highlighted in green.

Push Force

Bore ϕ mm	Bore Area sq. mm	Cylinder Push Force in kN						
		10 bar	40 bar	63 bar	100 bar	125 bar	160 bar	210 bar
25	491	0.5	2.0	3.1	4.9	6.1	7.9	10.3
32	804	0.8	3.2	5.1	8.0	10.1	12.9	16.9
40	1257	1.3	5.0	7.9	12.6	15.7	20.1	26.4
50	1964	2.0	7.9	12.4	19.6	24.6	31.4	41.2
63	3118	3.1	12.5	19.6	31.2	39.0	49.9	65.5
80	5027	5.0	20.1	31.7	50.3	62.8	80.4	105.6
100	7855	7.9	31.4	49.5	78.6	98.2	125.7	165.0
125	12272	12.3	49.1	77.3	122.7	153.4	196.4	257.7
160	20106	20.1	80.4	126.7	201.1	251.3	321.7	422.2
200	31416	31.4	125.7	197.9	314.2	392.7	502.7	659.7

Figure 3.22: Push force [32]

Deduction for Pull Force

Piston Rod ϕ mm	Piston Rod Area sq. mm	Reduction in Force in kN 10 bar	40 bar	63 bar	100 bar	125 bar	160 bar	210 bar
12	113	0.1	0.5	0.7	1.1	1.4	1.8	2.4
14	154	0.2	0.6	1.0	1.5	1.9	2.5	3.2
18	255	0.3	1.0	1.6	2.6	3.2	4.1	5.4
22	380	0.4	1.5	2.4	3.8	4.8	6.1	8.0
28	616	0.6	2.5	3.9	6.2	7.7	9.9	12.9
36	1018	1.0	4.1	6.4	10.2	12.7	16.3	21.4
45	1591	1.6	6.4	10.0	15.9	19.9	25.5	33.4
56	2463	2.5	9.9	15.6	24.6	30.8	39.4	51.7
70	3849	3.8	15.4	24.2	38.5	48.1	61.6	80.8
90	6363	6.4	25.5	40.1	63.6	79.6	101.8	133.6
110	9505	9.5	38.0	59.9	95.1	118.8	152.1	199.6
140	15396	15.4	61.6	97.0	154.0	192.5	246.3	323.3

Figure 3.23: Deduction for pull force [32]

Table 3.5: Cylinder pull force

Bore Ø [mm]	Piston rod Ø [mm]	Cylinder Pull Force [kN] 10 bar	40 bar	63 bar	100 bar	125 bar	160 bar	210 bar
25	45	-1.1	-4.4	-6.9	-11.0	-13.8	-17.6	-23.1
40	45	-0.3	-1.4	-2.1	-3.3	-4.2	-9.8	-7.0
50	45	0.4	1.5	2.4	3.7	4.7	-0.9	7.8
63	45	1.5	6.1	9.6	15.3	19.1	24.4	32.1
80	45	3.4	13.7	21.7	34.4	42.9	37.3	72.2
100	45	6.3	25.0	39.5	62.7	78.3	72.7	131.6
125	45	10.7	42.7	67.3	106.8	133.5	170.9	224.3
160	45	18.5	74.0	116.7	185.2	231.4	296.2	388.8
200	45	29.8	119.3	187.9	298.3	372.8	477.2	626.3

Upon further examination of the Table 3.5, it was determined that, while various diameter-pressure combinations are feasible, a balanced combination was chosen, with no excessively high pressures or enormous diameters. To avoid a cylinder that was too heavy, a bore diameter of 63 mm and a pressure of 100 bar was used instead of 80 mm and 63 bar.

After determining the diameter, it was needed to ascertain whether support was required for the required stroke. Figure 3.24 shows that with an end mounting support, a 1500 mm stroke may be achieved without the need for any further support, hence no more support was required in this circumstance.

Maximum Stroke Lengths of Unsupported Cylinders (in mm)

Bore Ø	Intermediate Mounting	End Support Mounting
25, 32, 40	1500	1000
50, 63, 80	2000	1500
100, 125	3000	2000
160, 200	3500	2500

Figure 3.24: Maximum stroke lengths of unsupported cylinders [mm] [32]

Another consideration is whether or not cushing is required. When piston speeds exceed 0.1 m/s and the piston will complete a full stroke, this is suggested. Because neither of these things occurs, it was decided that this would not be included in the cylinder.

Tie rods may have a bracket to increase the resistance to buckling of long-stroke cylinders, but for the desired bore diameter and stroke, no bracket is required, as shown in Figure 3.25.

Bore Ø	Stroke (meters)												No. of Supports Required
	0.9	1.2	1.5	1.8	2.1	2.4	2.7	3.0	3.3	3.6	3.9	4.2	
25	1	1	2	Consult Factory									
32	-	1	1	2									
40	-	-	1	1	1	2	2						
50	-	-	-	1	1	1	2	2	2	2	2	3	
63	-	-	-	-	-	1	1	1	1	1	2	2	
80	-	-	-	-	-	-	-	1	1	1	1	1	
100	-	-	-	-	-	-	-	-	-	1	1	1	

Figure 3.25: Number of tie rod supporters needed [32]

The reference number for the desired hydraulic cylinder is HMI-220626130504516. Appendix 3.26 contains a summary report on this hydraulic cylinder. Figure 3.26 shows the 3D model of the chosen cylinder.

Figure 3.26: 3D model of HMI-220626130504516 hydraulic cylinder [33]

It can be seen that it is necessary to add accessories to it to assemble it in the machine. For this purpose, an eye bracket was added on the left side of the hydraulic cylinder that allows the attachment of the tip to the base bar. The chosen model was based on the size of the connecting shaft that is attached to the cylinder. As it was 36 mm this model was chosen for having the hole with the same diameter. In addition, this model has a load capacity of 125 kN, so it is more than capable of withstanding the force required of it. For the right-hand end of the hydraulic cylinder, as it has a 33 mm end, the plain rod eye was chosen with an entry with the same diameter and the corresponding pivot pin and clevis bracket. Note that these components also have a load capacity of 125 kN.

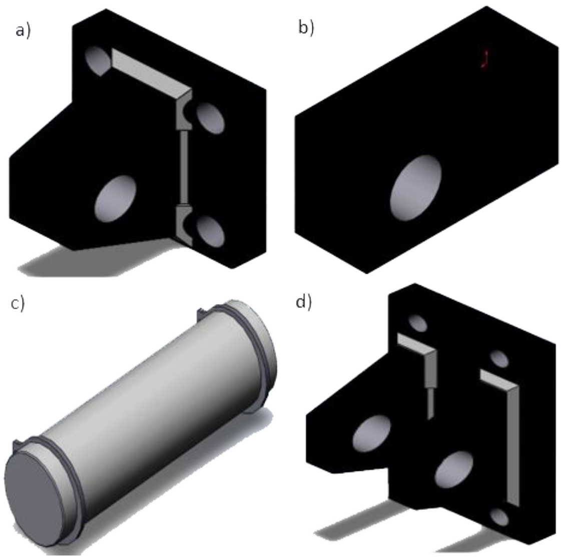

Figure 3.27: 3D model of the components: a) eye bracket b) plain rod eye c) pivot pin d) clevis bracket [34]

3.6.5 Power Unit

To have a working hydraulic cylinder it is necessary to have a power unit associated with it. This type of equipment is mostly composed by a motor, a reservoir and a hydraulic pump.

These systems vary greatly in terms of power, oil storage capacity, size, among others, so it is necessary to dimension them for each specific case.

To begin with, a compact power unit was chosen since it allows the hydraulic cylinder to function correctly while occupying a much smaller space than a normal hydraulic power pack. At the same time, they are easier to maintain since they use fewer moving parts as compared to mechanical systems, and have fewer leak points, making them more economical, safer, and simpler. Therefore, a compact Bucher UP series unit was selected, more specifically the UP50 model, as it is the only reversible unit with a tank of sufficient capacity [35].

To start the selection of the different components it is necessary to determine the amount of oil required for the cylinder to travel the entire stroke, that is, to calculate the maximum volume of the cylinder.

For a cylinder with a diameter of 63 mm and a stroke of 620 mm, a volume of 1.932 dm^3 was obtained. Given this, a tank with a capacity of 4 L was selected because some portion of oil needs to remain in the tank at all times. In addition, a tank with the filler at the front and drain outlet was opted for so that, should the need arises, the oil can be removed from inside the tank (see Appendix E.1). As for its assembly, due to the available space, it was decided to assemble it horizontally, more specifically in position P01 (see Appendix E.2).

The second step was to analyse the maximum flow rate. As mentioned in Chapter 3.1, the maximum velocity is 1º/s. As the calculations are being made for a maximum elevation of 45º, it is known that at the maximum, the cylinder has to travel the 620 mm in 45 s. That is, this translates to a velocity of 13.778 mm/s which corresponds to a maximum flow rate of 0.043 dm^3/s or 2.577 L/min.

Having this information, the different gear pumps options that the supplier has available for the reversible model (see Appendix E.3) were analysed and the flow rate, torque, and power of each one were calculated in order to select the most suitable one (see Table 3.6). For this, Equations 3.13, 3.14, 3.15 and 3.16 were used, which were taken from the equipment catalog [36]. It should be noted that the efficiencies assumed were those provided in the supplier's example calculation in the catalog.

$$Q = \frac{V_c \times n}{100000} \times \eta_v \tag{3.13}$$

$$\eta_t = \eta_v \times \eta_m \tag{3.14}$$

$$N = \frac{Q \times O}{6 \times \eta_t} \tag{3.15}$$

$$M = 9555 \times \frac{N}{n} \tag{3.16}$$

Where:

V_c: Pump displacement [cm^3/rev];

n: Drive shaft [rev/min];

Q: Flow rate [L/min];

O: Operating pressure [bar];

M: Torque [Nm];

N: Power [kW];

η_v: Volumetric efficiency [%];

η_m: Mechanical efficiency [%];

η_t: Total efficiency [%].

Table 3.6: Gear pumps calculations

V_c [cm^3/rev]	n [rev/min]	Q [L/min]	N [kW]	M [Nm]
0.25	3000	0.71	0.14	0.46
0.5	3000	1.41	0.29	0.91
0.75	1500	1.06	0.21	1.37
0.9	1500	1.27	0.26	1.64
1.2	1500	1.70	0.34	2.19
1.6	1500	2.26	0.46	2.92
2.3	1500	3.24	0.66	4.20

After reviewing this results, it was decided that the engine with a displacement of 2.3 cm^3/rev would provide the best flow rate without being too slow.

As for the type of motor, since its application will be stationary one can choose an alternating current (AC) electric motor. Also, these motors are cheaper than direct current (DC) motors which makes them preferable. From the supplier [35], for intermittent use (S3), there is only one option which is a three-phase motor with a power of 0.75 kW (see Appendix E.4). As for its support, it was decided to choose the B34 frame to ensure more stability.

To ensure that the pressure does not greatly exceed the maximum pressure, it was decided to add a pressure relief valve limited to 130 bar (see Appendix E.5).

As for the power pack housing, the K50 model was chosen (see Appendix E.6) due to the fact that it allows for a reversible circuit. The chosen preassembled housing, which also includes the shaft seal, was the model with the reference number: 200740250110.

For the drive, the E31 (see Appendix E.7) was chosen because it is suitable for three-phase AC motors and has the required power.

To ensure the desired movement of the system, one has to take advantage of the properties of a solenoid valve between the power unit and the control pendant that allows the user to regulate the up and down movements of the platform. A normally closed valve was chosen to guarantee that when the power unit is switched on, the oil does not immediately start to flow into the cylinder (see Appendix E.8).

In addition to this valve, it is also necessary to install a mechanical pilot operated valve - VRP05 (see Appendix E.9) - to guarantee a correct and functional hydraulic circuit.

3.6.6 Fork-Shaft Assembly

The rotation of the structure's top is enabled by the presence of two shaft-fork assemblies, which consist of the fork, the shaft, a bearing attached to the structure's base, two screws that attach the assembly to the structure's top, and a screw that prevents the shaft from rotating.

3.6.6.1 Ball Bearing Unit

From the initial calculations it was estimated that the forces that each bearing has to withstand correspond to half the force of the supports. That is, for dimensioning, each bearing must support an axial force of 4447.2 N and a radial force of 3.3 N. Following SKF recommendations for bearing sizing the following calculations were made.

$$P_0 = X_0 \times F_r + Y_0 \times F_a \tag{3.17}$$

Where:

P_0: equivalent static bearing load [N];

X_0: radial load factor for the bearing;

F_r: radial bearing load [N];

Y_0: axial load factor for the bearing;

F_a: axial bearing load [N].

It is known that for single row radial ball bearings X_0=0.6 and Y_0=0.5 [37]. Substituting this in Equation 3.17 gives a P_0 = 2225.6 N.

The static load rating C_0 is given by Equation 3.18 [37].

$$C_0 = s_0 \times p_0 \tag{3.18}$$

Where:

C_0: required basic static load rating [N];

s_0: static safety factor.

Solving Equation 3.18 and considering a safety factor of 1.5 resulted in a C_o of 3338.411 N.

The equivalent dynamic bearing load P is given by Equation 3.19.

$$P = X \times F_r + Y \times F_a \tag{3.19}$$

Where:

P: equivalent dynamic bearing load [N];

X: radial load factor for the bearing;

Y: axial load factor for the bearing.

The value of X and Y vary according to whether the ratio of axial force to radial force is greater or less than the axial load factor e. For the present case e is given by Equation 3.20 [37].

$$e = 0.28 \times [(15 \times F_a)/C_0]^{0.23} \tag{3.20}$$

The ratio of axial force to radial force is 12.445 which means that is greater than e so X = 0.56 and Y = $\frac{0.44}{e}$ = 0.789. Substituting in 3.19, P = 3511.289 N.

The dynamic load rating C is given by Equation 3.21 [37].

$$C = \frac{f_l}{f_n \times f_t} \times P \tag{3.21}$$

Where:

f_l: dynamic stress factor;

f_n: speed factor;

f_t: temperature factor;

Y: axial load factor for the bearing.

Since the number of revolutions per minute is very low and the machine environment does not reach very high temperatures f_t = 1 was considered, according to Table 3.7.

Table 3.7: Average values for the temperature factor [f_t] [38]

Maximum service temperature [ºC]	**< 120**	**up to 200**	**up to 250**	**up to 300**
Temperature factor [f_t]	1.0	0.73	0.42	0.22

The speed factor and the dynamic stress factor were taken from [38] as per the information provided in the literature. An f_n of 1.49 and an f_l of 3 were considered.

Solving Equation 3.21, by substituting the known values, resulted in a C = 7069.7 N.

The values obtained for the C and the C_0 load rating correspond to the minimum that the bearing must guarantee, so the selected bearing must have a dynamic and static load rating equal to or greater than those mentioned before.

Considering the movement to which the bearing is subjected, it makes no sense to calculate the bearing's life.

Looking at the SKF pillow block units it was found that one could choose one with a diameter of 12 mm but a larger diameter, 20 mm, was chosen because of the inability of the shaft to support the stresses and loads applied to it with such a small diameter for the required length.

The pillow block unit chosen was the P 20 RM (see Fig.3.28). It has a 20 mm internal diameter ball bearing and a stamped steel bearing. Its characteristics are presented in Appendix F.

Figure 3.28: Pillow block unit P 20 RM

3.6.6.2 Shaft

The shaft is essentially subjected to bending and shear stresses, so the torsion calculation was not performed.

To begin the calculations, the resultant force in the support (bearing) and the maximum bending moment were calculated. Figure 3.29 represents a simplification of the forces applied on the shaft.

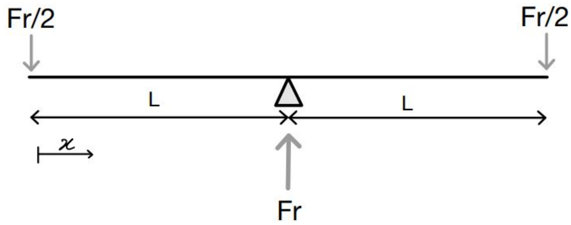

Figure 3.29: Diagram of the forces applied to the shaft

$$F_r = \sqrt{R_{ax}^2 + R_{ay}^2} \tag{3.22}$$

$$M_f(x) = -0.5 \times F_r \times x + (x - L) \times F_r \tag{3.23}$$

Analysing Equation 3.23, it is verified that the maximum bending moment occurs when x=L for x between L and 2L .

For the bending calculation, the Soderberg Equation 3.24 was used, for which it was necessary to determine certain parameters using Equations 3.25 to 3.28.

$$\frac{K_f \times \sigma_a}{\sigma_{fo}^c} = \frac{1}{C.S} \tag{3.24}$$

$$\sigma = \frac{32 \times M_f}{\pi \times d^3} \tag{3.25}$$

$$\sigma_a = \frac{\sigma_{max} + \sigma_{min}}{2} = \sigma \tag{3.26}$$

$$\sigma_{fo} = 0.5 \times \sigma_r \tag{3.27}$$

$$\sigma_{fo}^c = C_1 \times C_2 \times C_3 \times \sigma_{fo} \tag{3.28}$$

Where:

F_r: Resulting force [N];

M_f: Bending moment [Nmm];

K_f: Fatigue stress concentration factor;

d: Shaft diameter [mm];

σ: Bending stress [MPa]

σ_a: Stress amplitude [MPa];

σ_{fo}^c: Corrected fatigue limit stress [MPa];

σ_{fo}: Fatigue limit stress [MPa];

C.S.: Safety coefficient;

C_1: Load type factor;

C_2: Size effect factor;

C_3: Surface finish factor.

The value of L was varied in order to have a C.S. greater than 1.5.
Table 3.8 displays the chosen/calculated values for the necessary constants.

Table 3.8: Selected / calculated values for the required constants

	K_f	C_1	C_2	C_3
Values	1	1	0.900	0.835

In the end, it was decided for a L = 26 mm which translates into a shaft length of 72 mm and a diameter of 20 mm.

To examine the influence of pure shear on the shaft, the Tresca criteria was considered to determine the maximum shear stress that exists in the shaft. For that, Equations 3.29 and 3.30 were used.

$$\tau_{max} = \sqrt{(\frac{\sigma}{2})^2 + \tau_{nom}^2} \tag{3.29}$$

$$\tau_{nom} = \frac{F_r/2}{\pi \times d^2/4} \tag{3.30}$$

$$\tau_{max} \leq \frac{\sigma_y}{2 \times C.S.} \tag{3.31}$$

Where:

τ_{max}: Maximum shear stress [MPa];

τ_{nom}: Nominal shear stress [MPa];

d: Shaft diameter [mm];

F_r: Resulting force [N];

σ_y: Yield stress [MPa];

C.S.: Safety coefficient.

A maximum shear stress of 37.4 MPa was obtained for the shaft with the dimensions mentioned above. This result validates Equation 3.31 and, as a result, demonstrates that the shaft can be used in the predicted situation.

3.6.6.3 Fork

After deciding on the shaft and bearing, the next step was to determine the dimensions of the fork.

The support length on each side of the shaft was calculated to be equal to the shaft diameter, and the depth was calculated to be twice the shaft diameter. The total length was calculated by adding the chosen bearing's side length to twice the shaft support length.

Figure 3.30 depicts the geometry of the fork.

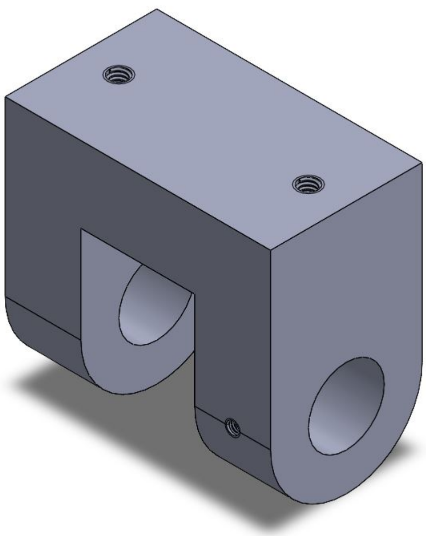

Figure 3.30: Three-dimensional model of the fork

3.6.6.4 Main Screw

To fix the fork to the underside of the platform, welding was initially considered, but this idea was discarded because it could create warping that would become detrimental to the rotation of the system. Therefore, it was decided to use two screws to fix it.

By analysing the rotation movement of the platform it is possible to verify that I works as a fictitious joint and causes a stress point, so it is necessary to take this point into account when dimensioning the screws (see Figure 3.31). Using Equations 3.32, 3.33, 3.34, 3.35 and 3.36 it is possible to take this into account.

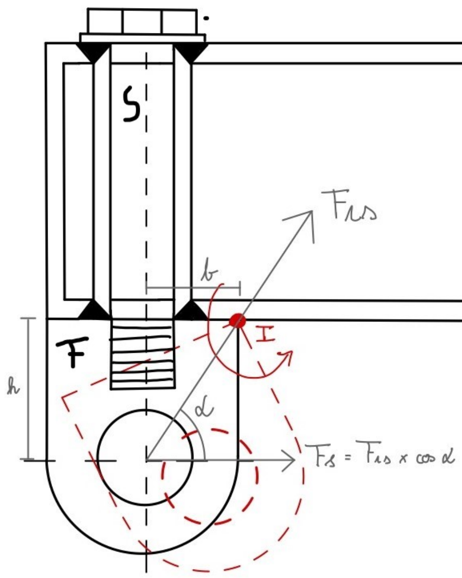

Figure 3.31: Sketch of the forces acting on the screw: P- Platform, S- Screw, F- Fork

$$F_{rs} = \frac{F_r}{2} \tag{3.32}$$

$$F_s = F_{rs} \cos(\alpha) \times \frac{h}{b} \tag{3.33}$$

$$A_{min} = \frac{\pi}{4} \times (d_1 - 0.935 \times Pt)^2 \tag{3.34}$$

$$d_1 = d_t - 1.0825 \times Pt \tag{3.35}$$

$$\sigma_s = \frac{F_s}{A_{min}} \leq 0.75 \times \sigma_{ys} \tag{3.36}$$

Where:

F_{rs}: Force acting on each screw [N];

F_s: Screw force [N];

α: Platform rotation angle [º];

h: Vertical distance between the center of the bore hole and I [mm];

b: Horizontal distance between the center of the bore hole and I [mm];

A_{min}: Minimum resistant section area [mm^2];

d_1: Smallest thread diameter [mm];

Pt: Pitch [mm];

d_t: Largest thread diameter [mm];

σ_{ys}: Yield stress of the screw [MPa];

σ_s: Resulting screw stress [MPa].

To verify which bolt was best, calculations were performed for different bolt sizes and the results shown in Table 3.9 were obtained. Note that a class 8.8 bolt was chosen, i.e. it has a yield strength of 800 MPa.

Table 3.9: Force supported by the screw according to its size

M	**P**	**d_{min} [mm]**	**L_{max} [mm]**	**A_{min} [mm^2]**	**σ_s [MPa]**
1.6	0.35	1.22	16	0.63	43844.68
2	0.4	1.57	20	1.12	2461.56
2.5	0.45	2.01	25	1.99	1382.09
3	0.5	2.46	30	3.11	883.57
3.5	06	2.85	35	4.12	668.36
4	0.7	3.24	40	5.26	523.18
5	0.8	4.13	50	9.00	305.58
6	1	4.92	60	12.46	220.89
8	1.25	6.65	80	23.57	116.74
10	1.5	8.38	100	38.20	72.04
12	1.75	10.11	120	56.34	48.84
14	2	11.84	140	77.99	35.28
16	2	13.84	160	112.44	24.47
18	2.5	15.29	180	131.84	20.87
20	2.5	17.29	200	175.69	15.66
22	2.5	19.29	220	225.81	12.19
24	3	20.75	240	252.99	10.88

Given the way the assembly is done, it is known that the screw must be longer than 40 mm and shorter than 67 mm. Only from M5 onwards is it possible to comply with this range.

An M6 bolt was selected because it allows for a longer length, and therefore better fastening, while ensuring that the stress to which it is subjected does not exceed the yield stress. The surface of the screw is galvanized steel since it is subject to possible oxidation due to possible contact with water and oil.

It should be noted that only one screw was needed to secure the components, but for the sake of symmetry and to give a greater sense of security and better fastening, it was decided to use two.

3.6.6.5 Bushing

This component (see Fig. 3.32) serves only to guide the screws when they pass through the profile and will be applied to the fork and pillow block unit screws.

In both situations, the bushing will have an internal diameter of 8 mm and a thickness of 4 mm. As for the length, since the profiles in both situations have different heights, they differ: 50 mm for the pillow block unit and 40 mm for the other.

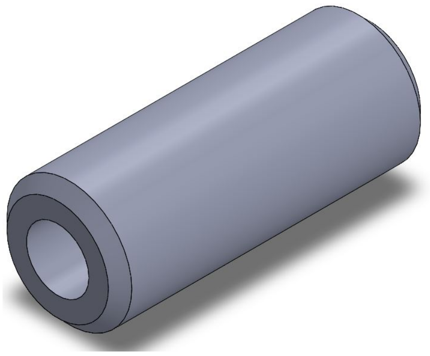

Figure 3.32: Bushing

3.6.6.6 Knurled Cup Socket Set Screw

The knurled cup socket set screw serves to secure the shaft to the fork so that it is immobilized.

An M4 with a length of 10 mm was selected because this is the available length between the surface of the shaft and the end of the fork.

3.6.7 Test Area

Since the machine allows tests on different floor types it has to be possible to change the test area easily, quickly and without temporary and/or permanent damage to the structure. Therefore, it was decided to create 3 fixation bars (see Figure 3.33) that are on three sides of the floor under test in order to keep it fixed.

Initially it was considered to weld the bars to the base of the machine, however, this permanent fixation made it harder to clean the machine between tests and would make it more difficult to replace the floor. Thus, it was decided to fix the bars with ISO 4014 hex-head screw - M6x30 - 8.8 screws that go through the base and are secured with a nut.

The two side bars are 1000 mm long, 20 mm wide, and 5 mm thick. The end bar has the following dimension 540 x 20 x 5 mm. In both models, the fastening is done at both ends.

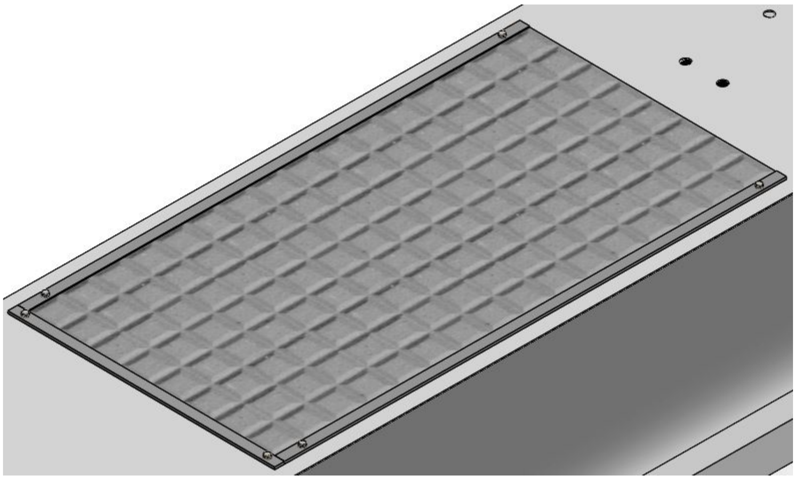

Figure 3.33: Three-dimensional model of the fixation bars

As a structural precaution, to ensure that the two screws that secure the end bar do not shear, it is suggested that they have a preload fastening. That is, this is so that the maximum clamping force of the bolts prevents sliding due to friction.

Next, the calculations for determining the clamping force of each screw are presented and it is checked whether it is sufficient to ensure that no slippage occurs.

Required screw dimensions:

ϕ Screw = 6 mm

ϕ Screw head = 6.8 mm

A_{min} = 18.996 mm^2

r_{avg} = 6.4 mm

$$Cf = \sigma_{preload} \times A_{min} \tag{3.37}$$

$$M_t = Cf \times \mu \times r_{avg} \tag{3.38}$$

Where:

Cf: Clamping force [N];

$\sigma_{preload}$: Preload tension [MPa];

A_{min}: Minimum resistant section area [mm^2];

M_t: Tightening torque [Nmm];

μ: Coefficient of friction;

r_{avg}: Average screw radius.

Substituting the values and considering a preload stress of 480 MPa and a coefficient of friction of 0.3, a clamping force of 9118.1 N and a clamping torque of 17506.7 Nmm were obtained.

As mentioned earlier, it was considered that the tester can weight up to 2000 N. For this situation, it was found that the maximum force it can perform is 28828.43 N, which occurs when the platform makes a 45° angle with the ground. This means that each screw has to withstand a force of 1414.2 N.

Therefore, the force that each screw holds before slipping is equal to its clamping force times the coefficient of friction, which will be 2735.4 N. This value is much higher than the 1414.2 N, so performing this preloading operation ensures that the screws never shear off.

3.6.8 Levelling Feet

To ensure a balanced machine assembly even if the floor on which it is placed is not, it is necessary to use leveling feet such as the one in Figure 3.34.

Figure 3.34: Leveling foot

According to SolidWorks, the total mass of the machine is estimated to be 353 kg. Assuming the test person has a mass of 100 kg, the total mass that must be supported by the four supports is 453 kg. However, instead of dividing the mass by the four supports, it was divided by two, because when the platform is in its lifting motion, its centre of mass tends to the left, allowing the majority of the weight to be supported by only two levelling feet. As a result, each support must support at least 2265 N.

To fasten the leveling feet, square 40 x 40 x 10 mm plates with a 10 mm diameter threaded hole in the middle (see Figure 3.35) were welded to the base. These are used to increase the contact area to ensure that the nut, which holds the leveler at the desired height, does not go into the profile.

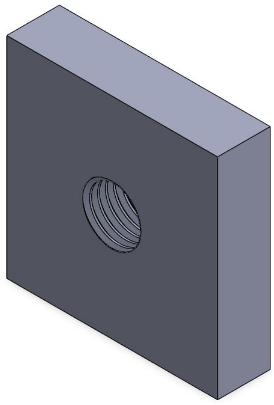

Figure 3.35: AISI 1024 steel plate with dimensions of 40 x 40 x 10 mm

As for the leveler, an M10 was chosen with a thread length of 30 mm that supports a load of 4 kN (see Appendix G). Note that by doing the Equation 3.12, referred to in Chapter 3.6.3, for an M6 foot leveler, a core tension of 131.6 MPa was obtained, i.e., one could have opted for a smaller leveler, however, to give a greater sense of safety and because the price difference between these two sizes is minimal, it was decided to choose the larger size.

3.6.9 Accessories

In addition to all these components, it is necessary to add a control pendant and a digital level.

The first is for the tester to regulate the raising and lowering of the platform as it moves along the test area. The control pendant should have three buttons: two that, respectively, when pressed cause the platform to go up or down until they remain active, and one that when pushed, in case of emergency, stops the functioning of the power unit.

The second serves to measure the elevation angle of the platform. This should be placed in such a way that the walker cannot see the value being measured.

3.7 Finite Element Analysis

In any project it is necessary to verify the structural stability. For that, in this case, ANSYS 2022 was used to perform this study.

Two types of tests were performed: one in which the mass of the tester of 100 kg at the center of the platform was considered, and another in which a descending force of 2000 N at the top of the harness was considered to simulate the moment when the tester slips and the harness holds it. In both cases, the base was considered fixed at the bottom and the rotation of the shaft of the fork-shaft assembly was enabled as shown in Figure 3.36. Note that for mesh simplification purposes the pillow block unit was replaced by a parallelepiped block. In addition, the platform can slide on the right side on the corresponding support.

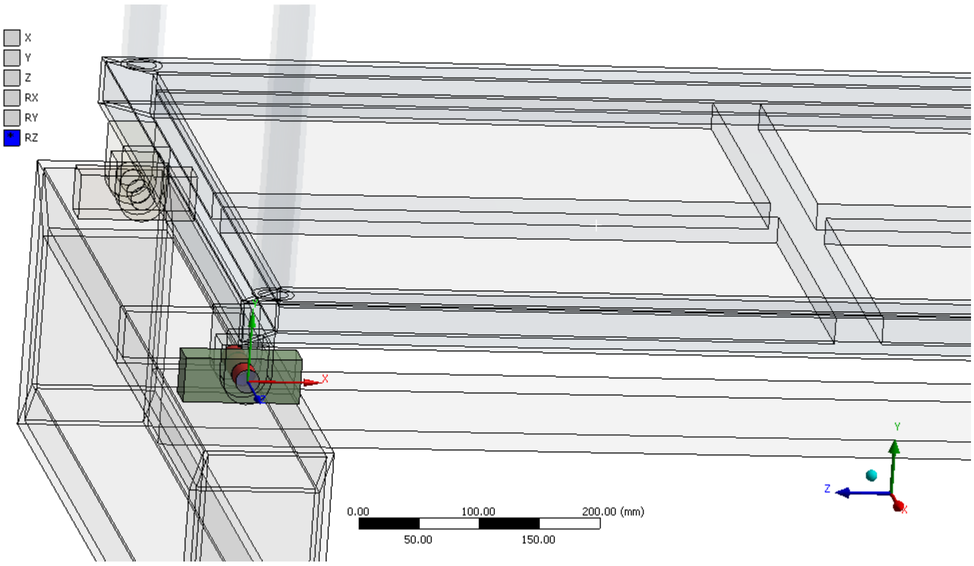

Figure 3.36: Shaft rotation movement

As for the mesh used, it is composed of tetrahedral elements, due to the complexity of the shapes that the complete structure presents. There were 149041 nodes and 78082 elements used in the mesh. Note that an attempt was made to simplify the structure by removing screws, nuts, washers, bushings, eyelets, and carabiners, among others, in order to facilitate the construction of the mesh without compromising the results.

In addition, the mesh was refined in two regions. At the rotation area (see Figure 3.37) and at the connection place of the harness components (see Figure 3.38) because they were zones that were predicted to be critical.

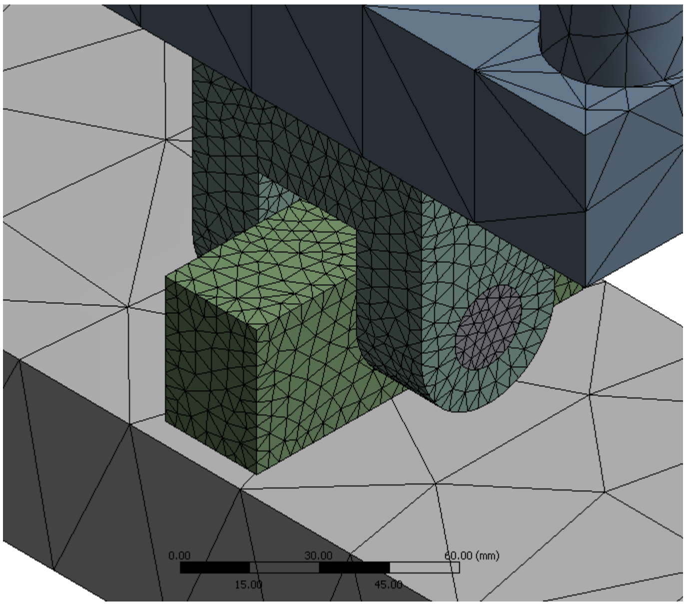

Figure 3.37: Detail of the mesh at the rotation point

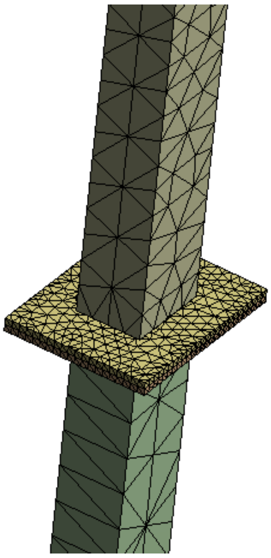

Figure 3.38: Detail of the mesh at the connection place of the harness components

Below, the results obtained for the two situations are shown.

3.7.1 Influence of the Tester

As mentioned earlier, the tester was considered to be in the middle of the platform in a 300 x 300 mm area to simulate the space it occupies. This simplification can be seen in Figure 3.39.

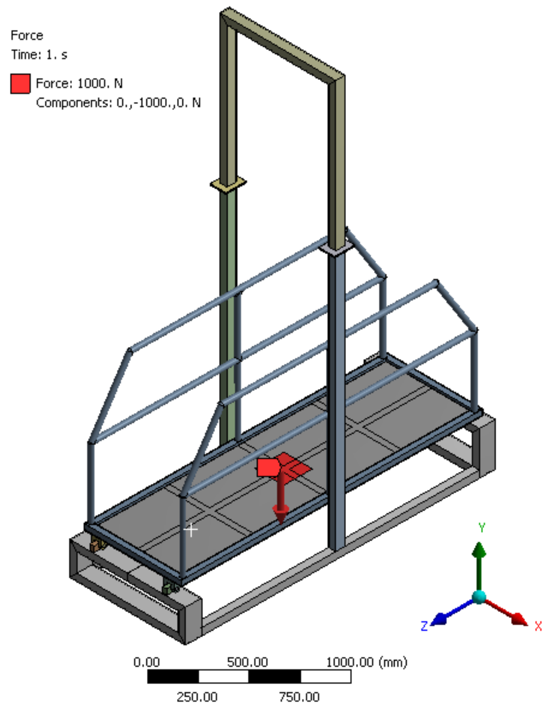

Figure 3.39: Load application in a 300 x 300 mm area

As would be expected, the vertical displacement reaches its maximum at the location of the force application and takes the value of 0.512 mm (see Figure 3.40), being this a very small result one can consider it as acceptable for the intended application.

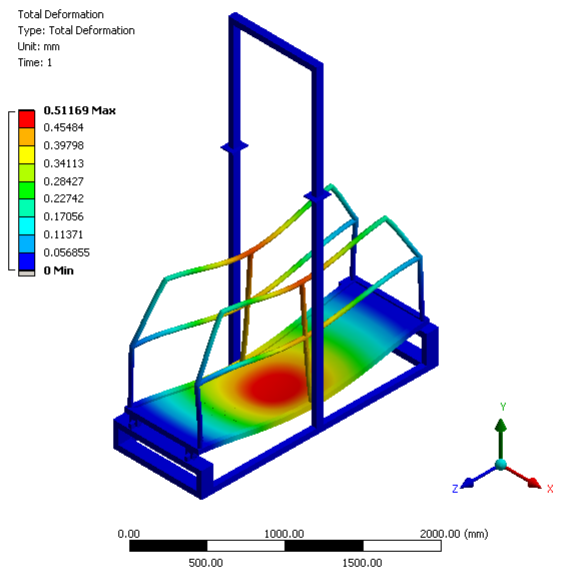

Figure 3.40: Displacement plot for a force of 1000 N

The handrail's corners experience the highest von Mises stress, which is 15.1 MPa (see Figure 3.41). Another important location is in the plate's support structure underneath the platform, as shown in Figure 3.42. Given that the material used for these components, AISI 1024, has a yield strength of 355 MPa it is possible to say that the structure will not yield and is stable, with a coefficient of safety of 23.6.

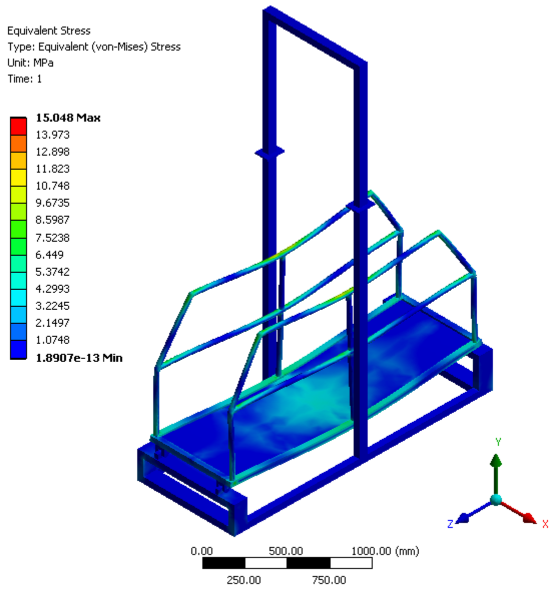

Figure 3.41: Von Mises stress plot for a force of 1000 N

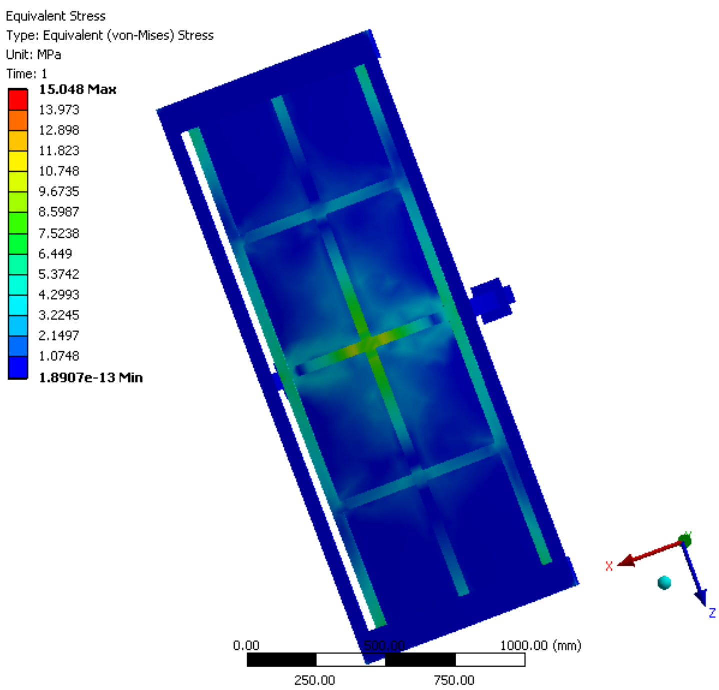

Figure 3.42: Von Mises stress plot for a force of 1000 N (bottom view)

3.7.2 Influence of the Tester's Fall

As mentioned in Chapter 3.7, for this test a vertical force of 2000 N was applied in an area of 65 x 50 mm, to the top bar of the harness support as shown in Figure 3.43.

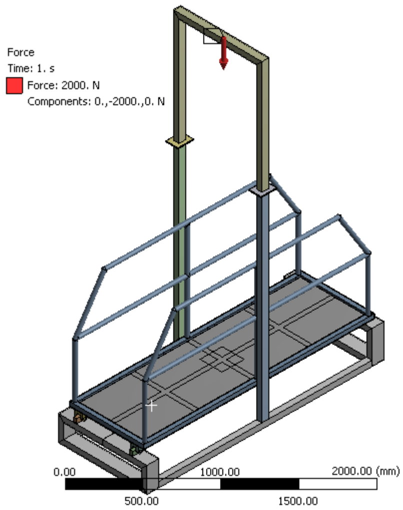

Figure 3.43: Load application of 2000 N in a 65 x 50 mm area

Proceeding to the analysis of Figure 3.44 it is observed a maximum deformation at the junction of the components of the harness structure of 0.254 mm. This value is even lower than in the previous test case, meaning that it is a good value that translates that the structure practically does not deform and is sufficiently rigid.

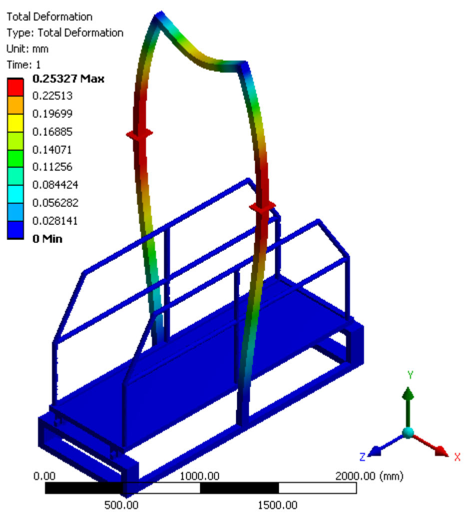

Figure 3.44: Displacement plot for a force of 2000 N in the safety harness support structure

Another analysis that was done was the von Mises stress (see Figure 3.45). Here it was found that the maximum stress occurs at the force application point and reaches the value of 21.1 MPa, again a much lower value than the yield strength of the AISI 1024 steel.

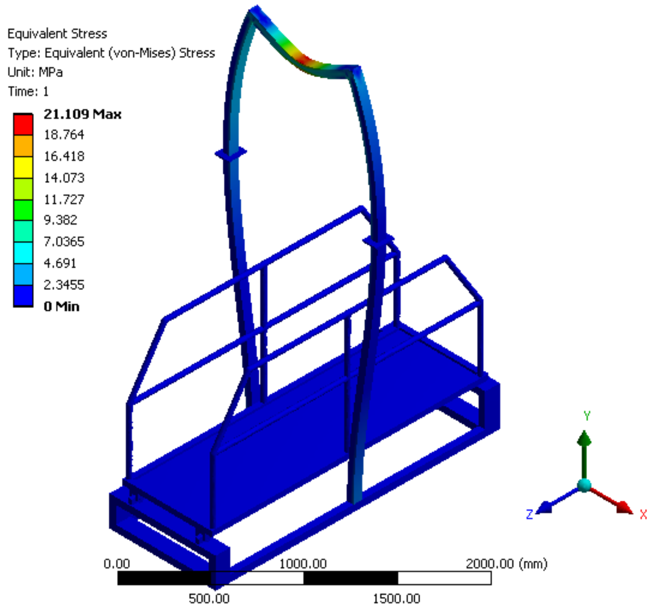

Figure 3.45: Von Mises stress plot for a force of 2000 N in the safety harness support structure

It is important to emphasize that the images are not presented at a 1:1 scale to highlight the behavior of the structure if a very high force was applied.

3.8 Conclusion

In conclusion, the different components were dimensioned using analytical elements and information from catalogs. In the various choices made during this process, the cost of the components was always taken into account so that in the future, if it is desired to build this machine, it can be done without a large investment. Taking into account the weight of the structure and the cost of materials and components, a total price of around 15 thousand euros was estimated.

At the end, a finite element analysis was performed to verify the structural health of the final project when applying the different loads to which it is subject.

Chapter 4

Conclusions and Future Work

This chapter highlights the final results found to meet the project's requirements and fulfill the specifications defined at the starting point, as well as future work that can be done to further improve the project.

4.1 Results

Currently, despite the use of safety shoes, many slips and falls still occur in workplaces due to low friction, especially when the floor is contaminated. In Portugal, this type of accident represents 15.5% [4] of the reported occupational work injuries. Therefore, the improvement of the methods of evaluation and study of shoes and floors has had a growing interest in both the footwear industry and the floor manufacturing industry.

As for the methods for doing these studies, there is a wide variety of equipment that evaluates the friction existing on the surfaces. The most widely used today, evaluate the coefficient of dynamic friction since most foot slips occur during foot movement [1]. Within these, they can be divided between those that use rubber to simulate the shoe sole and those that use shoes and allow the evaluation of different soles, including the study of the shoe thread effect. It is in the latter category that the ramp test comes in.

The Ramp Test follows the DIN 51130 standard and allows the study of different shoe-floor combinations when there is engine oil as a contaminant using a tester that walks along the test area while the test platform is raised to 40º.

Following this standard and the requirements it presents, the dimensioning of all the necessary components was done to obtain the complete design of the machine. By reviewing the operation of various lifting mechanisms currently available, it was found that the hydraulic cylinder is the best option for performing this movement and it was from there that the design process of the machine began.

Finally, it is reasonable to state that the main objective proposed was well achieved, since it was possible to design a test machine to evaluate the coefficient of friction between different safety shoes and types of floors, meeting the requirements of DIN 51130:2014-02. Furthermore, a more economically viable solution was obtained than the ones currently on the market, through a more detailed study of the required components for the desired movement, highlighting the employment of only one hydraulic cylinder instead of the common use of two and of a compact hydraulic unit. A total price of around 15 thousand euros was estimated considering the weight of the structure and the materials used in as the selected components. Additionally, a more space-efficient machine with smaller dimensions was achieved by allowing the rotation of the platform at one end of the support structure instead of at the center.

4.2 Further Work

Possible future developments might include creating a more automated system where the push of a button would begin to raise the platform and when it sensed a difference in movement, meaning when the tester slipped, the platform would descend slightly and rise again to check the angle of slippage. It may also include the addition of a tank of soapy water with a closed system for circulating it to cover this machine for studies of the DIN 51097 standard.

It is also suggested the study of the hypothesis of load cells under the test area to study the forces that the tester makes while walking in an attempt to hold himself and not slip, allied to this it would be interesting to have a monitoring system of the elevation angle in real time in order to obtain a more accurate result.

References

[1] James Hanson, Mark Redfern, and Mainak Mazumdar. Predicting slips and falls considering required and available friction. *Ergonomics*, 42:1619–33, 01 2000.

[2] Arian Iraqi, Rakié Cham, Mark S. Redfern, and Kurt E. Beschorner. Coefficient of friction testing parameters influence the prediction of human slips. *Applied Ergonomics*, 70:118–126, 2018.

[3] Kevin Hallas and Robert Shaw. Evaluation of the kirchberg rolling slider and slipalert slip resistance meters. 2006.

[4] Gabinete de Estratégia e Planeamento. *Acidentes de Trabalho*. 2019.

[5] Kurt Beschorner Taylor Jones, Arian Iraqi. Coefficient of friction of footwear with and without "slip-resistant" labels.

[6] April J. Chambers, Sarah Margerum, Mark S. Redfern, and Rakié Cham. Kinematics of the foot during slips. *Occupational ergonomics*, 3:225–234, 2002.

[7] James Clarke, Kevin Hallas, R. Lewis, S. Thorpe, Graeme Hunwin, and Matt Carré. Understanding the friction measured by standardised test methodologies used to assess shoe-surface slip risk. *Journal of Testing and Evaluation*, 43:20120334, 07 2015.

[8] Walter Pirker and Regina Katzenschlager. Gait disorders in adults and the elderly: A clinical guide. *Wiener klinische Wochenschrift*, 129, 10 2016.

[9] D.I. James. The theory behind the din ramp tests. *Polymer Testing*, 18(1):3–10, 1999.

[10] Kurt E. Beschorner and Gurjeet Singh. A novel method for evaluating the effectiveness of shoe-tread designs relevant to slip and fall accidents. *Proceedings of the Human Factors and Ergonomics Society Annual Meeting*, 56(1):2388–2392, 2012.

[11] Carita Aschan, Mikko Hirvonen, Tarmo Mannelin, and Erkki Rajamäki. Development and validation of a novel portable slip simulator. *Applied ergonomics*, 36:585–93, 10 2005.

[12] Seyed Reza Mirhassani Moghaddam. Computational models for predicting shoe friction and wear. Accessed on 2022-05-20, June 2018.

[13] Hisao Nagata. *Fall Prevention and Protection, Principles, Guidelines, and Practices*. 01 2017.

[14] Mark Redfern, Rakie Cham, Krystyna Gielo-Perczak, Raoul Grönqvist, Mikko Hirvonen, Håkan Lanshammar, Mark Marpet, Clive Pai, and Christopher Powers. Biomechanics of slips. *Ergonomics*, 44:1138–66, 11 2001.

[15] M.S. Redfern, A. Marcotte, and D.B. Chaffin. A dynamic coefficient of friction measurement device for shoe/floor interface testing. *Journal of Safety Research*, 21(2):61–65, 1990.

[16] A. Sariisik, S. Gurcan, and A. Senturk. Description of slipping test methods and application study on travertine by ramp slip meter. *Building and Environment*, 42(4):1707–1710, 2007.

[17] Munro Instruments. Ramp test vs pendulum. https://www.munroinstruments.com/ramp-test-vs-pendulum/, 2018. Accessed on 2022-04-19.

[18] Assessing the slip resistance of flooring. *Health and Safety Executive*, 2012.

[19] Mosa. Walking safety. https://www.mosa.com/application/files/3416/2332/0742/Walking-safety-info-sheet-Mosa.pdf, 2021.

[20] Sotter Engineering Corporation. Slip resistance testing standards in 2021. https://safetydirectamerica.com/slipresistancetestingstandards/, 2021. Accessed on 2022-04-19.

[21] Richard Bowman. Slip resistance testing - zones of uncertainty. *Boletín de la Sociedad Española de Cerámica y Vidrio*, 49, 07 2010.

[22] Skid Tester. Tortus 3 coefficient of friction tester. http://www.skid-tester.com/Tortus.html. Accessed on 2022-04-20.

[23] Murilo Scorisa, Ana Lot, F. Melchiades, and Anselmo Boschi. Breve descrição dos métodos de avaliação da resistência ao escorregamento de revestimentos cerâmicos. *Cerâmica Industrial*, 21:7–12, 05 2016.

[24] Floor Slip. Floor 'slip-alert' roller coaster floor tester. http://www.floorslip.co.uk/slip-resistance-testing.html. Accessed on 2022-04-20.

[25] SlipAlert. Slipalert results graph and conversion. http://www.slipalert.com/resources/graphs.htm, note = Accessed on 2022-04-20.

[26] G. Hunwin, Kirsty Ormerod, and Alison Darby. A study of the effect of modifying the european standard mechanical slip resistance test for footwear. 2010.

[27] P. J. PERKINS and M. P. WILSON. Slip resistance testing of shoes — new developments. *Ergonomics*, 26(1):73–82, 1983.

[28] Testing of floor coverings - Determination of the anti-slip property - Workrooms and fields of activities with slip danger - Walking method - Ramp test. Standard, Deutsches Institut für Normung, Berlin, Germany, February 2012.

[29] RAMADA AÇOS. St 52. https://www.ramada.pt/pt/produtos/acos/aa-os-de-construa-ao-ao-carbono/st-52_.html, 06 2018. Accessed on 2022-06-05.

[30] RAMADA AÇOS. F 10. https://www.ramada.pt/pt/produtos/acos/aa-os-de-construa-ao-ao-carbono/f10-.html, note = Accessed on 2022-06-05, 03 2018.

[31] RS Components. Mosquetón jsp far0902. https://pt.rs-online.com/web/p/mosquetones-de-seguridad/8610478. Accessed on 2022-05-20.

[32] Parker. Metric hydraulic cylinders - series hmi. https://www.parker.com/Literature/Industrial%20Cylinder/cylinder/cat/english/HY08-1151-2_NA_HMI.pdf. Accessed on 2022-05-27.

[33] Parker. econfigurator ™: Hmi cylinder. https://corpapps.parker.com/corpapps/CylinderConfigurator/home?mfgDivision=687744&mfglang=PT&mfgmod=HMI&selldivision=687744&option=64&ProductID=2390653&ProductURL=https://ph.parker.com/pt/pt/hmi-series-hydraulic-cylinders&ParentCatId=&LandingPageurl=http://ph.parker.com/pt/pt/ParkerExternalConfigCmds&series=HMI&JdeReferenceId=HMI-220626130504516. Accessed on 2022-05-20.

[34] Parker. Hmi accessories. https://corpapps.parker.com/corpapps/CylinderConfigurator//Resources/Accessories/HMI-accessories.html. Accessed on 2022-05-20.

[35] Bucher Hydraulics. Hydraulic power packs, series up. https://www.bucherhydraulics.com/47809/Products/Mobile-and-Industrial-Hydraulics/Products/Power-Units/Hydraulic-Power-Packs,-Series-UP/index.aspx?zfz=baadea86-0283-4eab-a8f8-761c1ba9a926. Accessed on 2022-05-20.

[36] Bucher Hydraulics. Hydraulic units up50. https://www.bucherhydraulics.com/datacat/files/Katalog/Hydroaggregate/Kompaktaggregate/040%20-%20UP50/UP50_200-P-991186-en.pdf. Accessed on 2022-05-20.

[37] Simões Morais. *Desenho técnico básico*. 12 2007.

[38] Francisco Q. de Melo António Completo. *Introdução ao Projeto Mecânico - 2ª edição*. 05 2019.

[39] Norelem. Mosquetón jsp far0902. https://norelem.es/medias/07680-Datasheet-4236-Parafusos-olhais-DIN-580-pt.pdf?context=bWFzdGVyfHJvb3R8MzAyND. Accessed on 2022-05-20.

[40] SKF. P 20 rm. https://www.skf.com/pt/products/mounted-bearings/ball-bearing-units/pillow-block-ball-bearing-units/productid-P%2020%20RM. Accessed on 2022-05-20.

[41] Norelem. 27794 pés niveladores redondos. https://norelem.es/medias/27794-Datasheet-22500-P-s-niveladores-redondos-pt.pdf?context=bWFzdGVyf. Accessed on 2022-05-20.

Appendix A

2D Drawings

Figure A.1: 2D drawing of the machine in the initial position

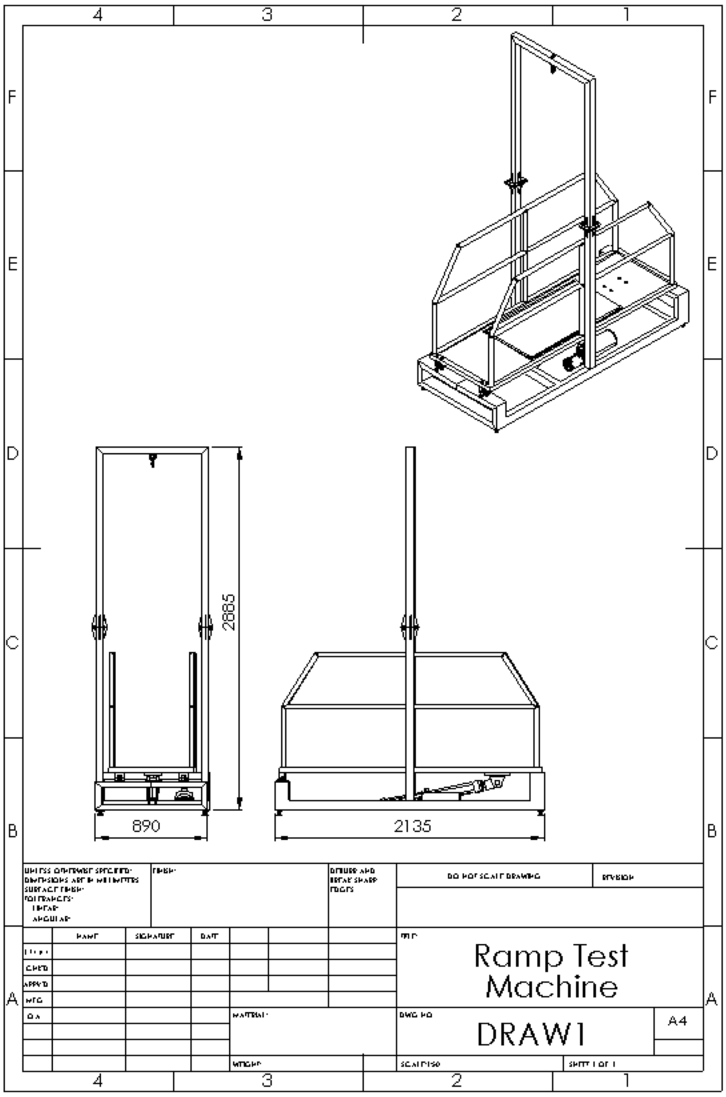

Figure A.2: 2D drawing of the machine in the final position

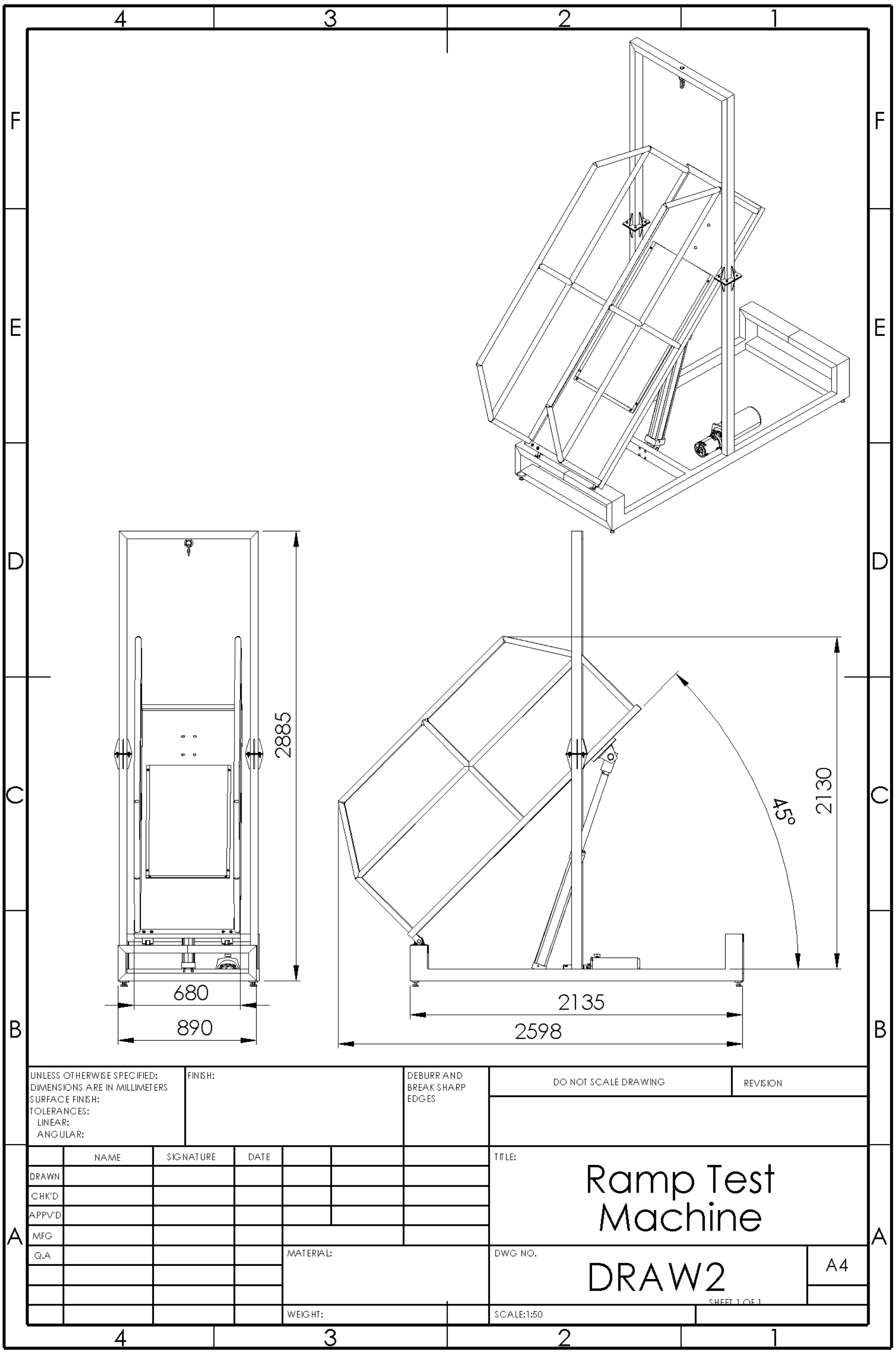

Appendix B

Material Data Sheets

B.1 AISI 1024

Figure B.1: Datasheet AISI 1024 steel - part 1 [29]

RAMADA AÇOS
SPECIAL STEEL SOLUTIONS

Bra-Azu-Bra

St 52
Aço construção carbono
W.Nr. 1.0553 / 1.0577

Normas:

EN: S 355 J0 / S 355 J2	AISI: (1024)	DIN: St 52-3 U
Fornecimento: EN 10025-2		

Estado de fornecimento:

Natural

Perfis disponíveis:

∅	Chapa
20 a 330 mm	8 a 120 mm
EN 10060	EN 10029

COMPOSIÇÃO QUÍMICA (%):

Aço	C	Si	Mn	P	S	Cu	N
S 355 J0	≤ 0,22	≤ 0,55	≤ 1,60	≤ 0,030	≤ 0,030	≤ 0,55	≤ 0,012
S 355 J2	≤ 0,22	≤ 0,55	≤ 1,60	≤ 0,025	≤ 0,025	≤ 0,55	---

CARACTERÍSTICAS:

Aço de construção não ligado que, sob os formatos essencialmente redondos e em chapa, tem um largo campo de aplicações, principalmente na construção soldada.

APLICAÇÕES PRINCIPAIS:

Todo o tipo de estruturas: componentes de pontes; gruas; componentes de plataformas; equipamentos mineiros de carga e para torres eólicas.

PROPRIEDADES:

Densidade: 7,80 Kg/dm³

Coeficiente de Dilatação Térmica, 10^{-6}m/mK:

20 a 600 °C	20 a 500 °C	20 a 400 °C	20 a 300 °C	20 a 200 °C	20 a 100 °C
---	---	---	---	---	16

Condutibilidade Térmica, W/mK:

400 °C	200 °C	20 °C
---	42,7	40

Módulo de Elasticidade, GPa:

600 °C	500 °C	400 °C	300 °C	200 °C	100 °C	20 °C	0 °C	-100 °C
---	---	---	---	---	---	200	---	---

Ramada Aços, S.A.
Avenida da Régua, Apartado 10, 3884-004 Ovar
Tel.: +351 256 580 580 | Fax: +351 256 580 500 / +351 256 580 410
www.ramada.pt | acos.ovar@ramada.pt

A informação fornecida é precisa e de confiança contudo, alguns dos valores apresentados são indicativos, não podendo possuir carácter vinculativo, dado existirem variações resultantes de erros associados aos ensaios e às actualizações documentais.
Data de Atualização: 27-06-2018

Figure B.2: Datasheet AISI 1024 steel - part 2 [29]

RAMADA AÇOS
SPECIAL STEEL SOLUTIONS

Bra-Azu-Bra

St 52
Aço construção carbono
W.Nr. 1.0553 / 1.0577

Propriedades Mecânicas:

Ø (mm)	Espessura (t) (mm)	Rm (MPa)	ReH (MPa)	A% (L0=5do)
≤ 16	≤ 16	470 – 630	≥ 355	≥ 22
≤ 40	≤ 40	470 – 630	≥ 345	≥ 22
≤ 63	≤ 63	470 – 630	≥ 335	≥ 21
≤ 80	≤ 80	470 – 630	≥ 325	≥ 20
≤ 100	≤ 100	470 – 630	≥ 315	≥ 20

Aconselhamento Técnico:
A nossa equipa técnica encontra-se disponível para esclarecimento de dúvidas e aconselhamento na selecção do material e tratamento térmico mais adequado à sua aplicação.

Ramada Aços, S.A.
Avenida da Régua, Apartado 10, 3884-004 Ovar
Tel.: +351 256 580 580 | Fax: +351 256 580 500 / +351 256 580 410
www.ramada.pt | acos.ovar@ramada.pt

Data de Atualização: 27-06-2018

B.2 AISI 1045

Figure B.3: Datasheet AISI 1045 steel- part 1 [30]

RAMADA AÇOS
SPECIAL STEEL SOLUTIONS

Branco

F 10
Aço construção ao carbono
W.Nr. 1.1191 / 1.1730

Normas:

EN: C45E / C45U	AISI: 1045	DIN: Ck 45
Fornecimento: EN 10083-1; EN 10083-2; EN 10250-2; EN ISO 4957		

Estado de fornecimento: Natural

Perfis disponíveis:

∅	▱	▭	Chapa	Plano
20 a 700 mm	20 a 100 mm	Espessuras: 6 a 120 Larguras: 20 a 2450 mm	Espessura: 3 a 12 mm	Espessura 125 a 455 mm
EN 10060	EN 10059	EN 10058	EN 10051	EN 10029-C/D

COMPOSIÇÃO QUÍMICA (%):

C	Si	Mn	P	S	Cr + Mo + Ni
0,42-0,50	<0,40	0,50-0,80	≤ 0,035	≤ 0,035	≤ 0,63

CARACTERÍSTICAS:

Aço de construção base para órgãos máquina e peças para metalomecânica que pode ser utilizado no estado natural de fornecimento ou então melhorado para espessuras mais baixas por tratamento térmico de têmpera ou carbonitruração. A nitruração favorecerá a resistência ao desgaste e à oxidação.

APLICAÇÕES PRINCIPAIS:

Orgãos de máquinas, veios, cavilhas, parafusos, porcas.

PROPRIEDADES:

Densidade: 7,84 Kg/dm³

Coeficiente de Dilatação Térmica, 10^{-6}m/mK:

20 a 600 ºC	20 a 500 ºC	20 a 400 ºC	20 a 300 ºC	20 a 200 ºC	20 a 100 ºC
14,7	14,2	13,7	13,1	12,3	11,6

Condutibilidade Térmica, W/mK:

400 ºC	200 ºC	20 ºC
---	---	15,1

Módulo de Elasticidade, GPa:

600 ºC	500 ºC	400 ºC	300 ºC	200 ºC	100 ºC	20 ºC	0 ºC	-100 ºC
---	---	---	---	---	---	200	---	---

Ramada Aços, S.A.
Avenida da Régua, Apartado 10, 3884-004 Ovar
Tel.: +351 256 580 580 | Fax: +351 256 580 500 / +351 256 580 410
www.ramada.pt | acos.ovar@ramada.pt

Data de actualização: 09/03/2018

Figure B.4: Datasheet AISI 1045 steel - part 2 [30]

RAMADA AÇOS
SPECIAL STEEL SOLUTIONS

Branco

F 10
Aço construção ao carbono
W.Nr. 1.1191 / 1.1730

TRATAMENTOS TÉRMICOS

	Temperatura	Meio de Arrefecimento	Dureza
Recozimento de Amaciamento	650-700 °C	Forno	≤ 207 HB
Têmpera	820-860 °C	Óleo	> 40 HRC
Nitruração	480-560ºC	---	> 250 HV1
Normalização	840-880 °C	---	≈ 220 HB
Redução de Tensões	550-600 ºC	---	---
Revenido	150-550 °C	Ar	---

DIAGRAMA TAC

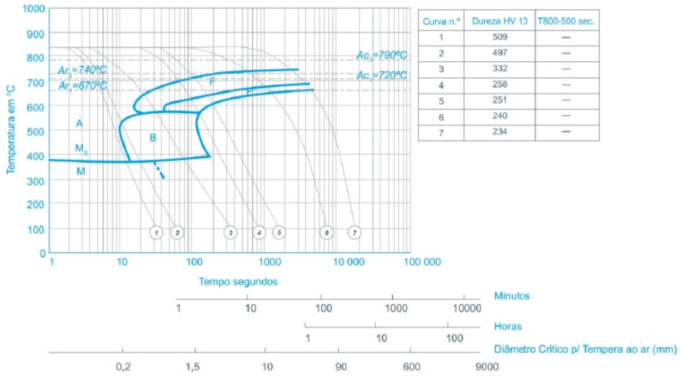

Curva n.º	Dureza HV 10	T800-500 sec.
1	509	---
2	497	---
3	332	---
4	258	---
5	251	---
6	240	---
7	234	---

CURVA DE REVENIDO

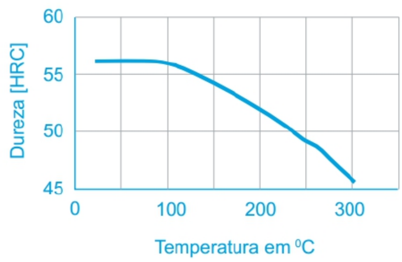

Aconselhamento Técnico:
A nossa equipa técnica encontra-se disponível para esclarecimento de dúvidas e aconselhamento na selecção do material e tratamento térmico mais adequado à sua aplicação.

Ramada Aços, S.A.
Avenida da Régua, Apartado 10, 3884-004 Ovar
Tel.: +351 256 580 580 | Fax: +351 256 580 500 / +351 256 580 410
www.ramada.pt | acos.ovar@ramada.pt

A informação fornecida é precisa e de confiança contudo, alguns dos valores são apresentados a título indicativo, não assumindo carácter vinculativo, dado a poder existir variações resultantes de erros associados aos ensaios e às fontes documentais.

Data de actualização: 09/03/2018

Appendix C

Safety harness support

C.1 Carabiner

Figure C.1: Technical specifications of the FAR0902 carabiner [31]

DOC NO	ISSUE	REVISION	PRODUCT REF.	DATE	QUALITY PLAN
QF/RD/05	01	00	FAR0902	18.09.14	

TECHNICAL SPECIFICATIONS	SIGNATURE PRESIDENT (TECHNICAL)

SCREW LOCKING STEEL KARABINER (FAR0902)

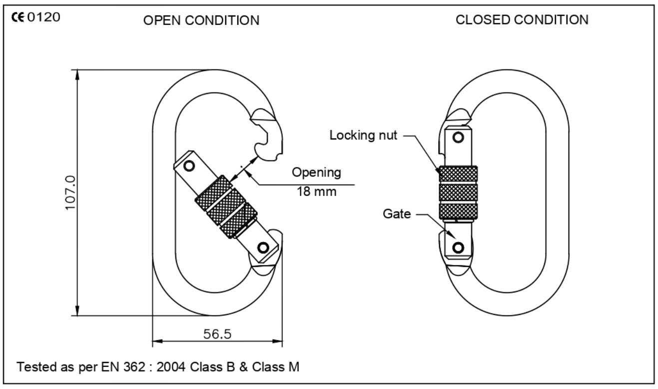

DESIGN	• Opening 18 mm. • Oval shaped Karabiner made of round Steel Bar. • Self closing & manual locking type Karabiner • Locking by screw locking nut
MATERIAL	• Alloy Steel.
FINISH	• Galvanized with Golden Yellow/Silver Passivation.
MINIMUM BREAKING STRENGTH	• 23 kN.
WEIGHT	• 160.5 gm ±10gm

JSP
OXFORD, ENGLAND

C.2 Eyebolt

Figure C.2: Datasheet of the chosen eyebolt [39]

07680 Parafusos olhais DIN 580

norelem

Descrição do artigo/Imagens dos produtos

Descrição

Material:
Aço cementado 1.1141, aço inoxidável 1.4301 ou aço inoxidável 1.4401.

Versão:
Estampado.
Aço com superfície sem proteção anticorrosiva.
Aço galvanizado com zinco.

Indicação:
Para atividades de elevação e carregamento com elevadas exigências em áreas relevantes para a segurança (engenharia mecânica, meios de suporte de cargas, meios de atamento e içamento de cargas).
A marcação CE está gravada no parafuso olhal.
A capacidade de carga F2 não deve ultrapassar 45° por parafuso olhal.

Sob consulta:
Certificado de conformidade.

Desenhos

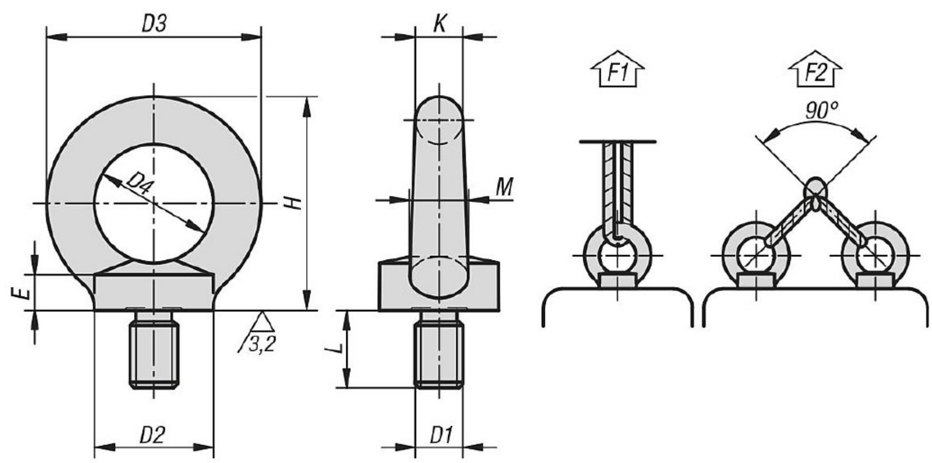

Visão geral dos artigos

Parafusos olhais DIN 580

Código do artigo	Material do corpo básico	Chave de aço	Superfície Corpo básico	D1	L	D2	D3	D4	E	H	K	M	F1 máx. kN	F2 máx. kN
07680-08	aço	1.1141	superfície sem tratamento	M8	13	20	36	20	6	36	8	10	1,4	0,95
07680-10	aço	1.1141	superfície sem tratamento	M10	17	25	45	25	8	45	10	12	2,3	1,7
07680-12	aço	1.1141	superfície sem tratamento	M12	20,5	30	54	30	10	53	12	14	3,4	2,4
07680-16	aço	1.1141	superfície sem tratamento	M16	27	35	63	35	12	62	14	16	7	5
07680-20	aço	1.1141	superfície sem tratamento	M20	30	40	72	40	14	71	16	19	12	8,3
07680-24	aço	1.1141	superfície sem tratamento	M24	36	50	90	50	18	90	20	24	18	12,7

 www.norelem.com 1/2

Appendix D

Hydraulic cylinder

D.1 Existing mounting styles

Figure D.1: Existing mounting styles for HMI series

Catalog HY08-1151-2/NA
Mounting Styles and Applications

Metric Hydraulic Cylinders
Series HMI

ISO Cylinder Mounting Styles

The standard range of Parker Series HMI cylinders comprises 12 ISO mounting styles, to suit the majority of applications. General guidance for the selection of ISO cylinders is given below, with dimensional information about each mounting style shown on the following pages. Application-specific mounting information is shown in the mounting information section on page 18.

Extended Tie Rods
Cylinders with TB, TC and TD mountings are suitable for straight line force transfer applications, and are particularly useful where space is limited. For compression (push) applications, cap end tie rod mountings are most appropriate; where the major load places the piston rod in tension (pull applications), head end mounting styles should be specified. Cylinders with tie rods extended at both ends may be attached to the machine member from either end, allowing the free end of the cylinder to support a bracket or switch.

Flange Mounted Cylinders
These cylinders are also suitable for use on straight line force transfer applications. Two flange mounting styles are available, offering either a head flange (JJ) or a cap flange (HH). Selection of the correct flange mounting style depends on whether the major force applied to the load will result in compression (push) or tension (pull) stresses on the piston rod. For compression-type applications, the cap mounting style is most appropriate; where the major load places the piston rod in tension, a head mounting should be specified.

Foot Mounted Cylinders
Style C, foot mounted cylinders do not absorb forces on their centerline. As a result, the application of force by the cylinder produces a moment which attempts to rotate the cylinder about its mounting bolts. It is important, therefore, that the cylinder should be firmly secured to the mounting surface and that the load should be effectively guided to avoid side loads being applied to rod gland and piston bearings. A thrust key modification may be specified to provide positive cylinder location.

Pivot Mountings
Cylinders with pivot mountings, which absorb forces on their centerlines, should be used where the machine member to be moved travels in a curved path. Pivot mountings may be used for tension (pull) or compression (push) applications. Cylinders using a fixed clevis, styles BB and B, may be used if the curved path of the piston rod travel is in a single plane; for applications where the piston rod will travel in a path on either side of the true plane of motion, a spherical bearing mounting SB is recommended.

Trunnion Mounted Cylinders
These cylinders, styles D, DB and DD, are designed to absorb force on their centerlines. They are suitable for tension (pull) or compression (push) applications, and may be used where the machine member to be moved travels in a curved path in a single plane. Trunnion pins are designed for shear loads only and should be subjected to minimum bending stresses.

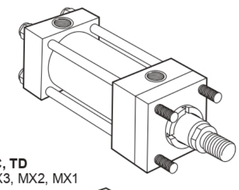

Styles TB, TC, TD
ISO Styles MX3, MX2, MX1 **TB**

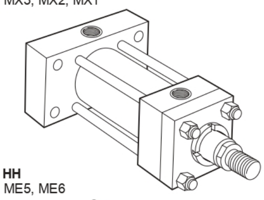

Styles JJ, HH
ISO Styles ME5, ME6 **HH**

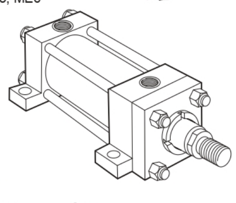

Style C
ISO Style MS2 **C**

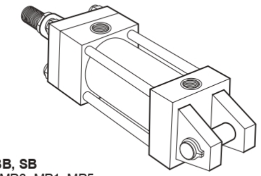

Styles B, BB, SB
ISO Styles MP3, MP1, MP5 **BB**

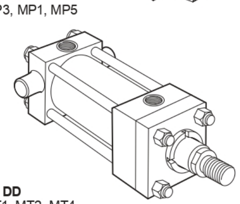

Styles D, DB, DD
ISO Styles MT1, MT2, MT4 **DB**

Parker
4
www.parker.com/cylinder
Parker Hannifin Corporation
Cylinder Division
Des Plaines, Illinois USA

D.2 Stroke factor

Figure D.2: Selection of the stroke factor

Catalog HY08-1151-2/NA
Stroke Factors

Metric Hydraulic Cylinders
Series HMI

Stroke Factors

The stroke factors below are used in the calculation of cylinder 'basic length' – see Piston Rod Size Selection.

Rod End Connection	Mounting Style	Type of Mounting	Stroke Factor
Fixed and Rigidly Guided	TB, TD, C, JJ	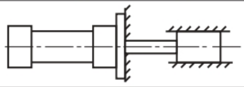	0.5
Pivoted and Rigidly Guided	TB, TD, C, JJ	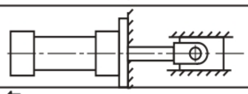	0.7
Fixed and Rigidly Guided	TC, HH	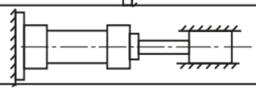	1.0
Pivoted and Rigidly Guided	D	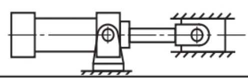	1.0
Pivoted and Rigidly Guided	TC, HH, DD	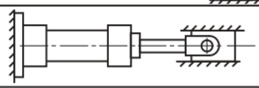 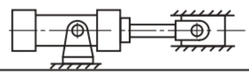	1.5
Supported but not Rigidly Guided	TB, TD, C, JJ	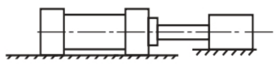	2.0
Pivoted and Rigidly Guided	B, BB, DB, SB	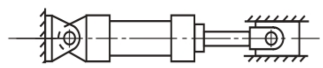	2.0
Pivoted and Supported but not Rigidly Guided	DD	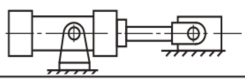	3.0

Long Stroke Cylinders

When considering the use of long stroke cylinders, the piston rod should be of sufficient diameter to provide the necessary column strength.

For tensile (pull) loads, the rod size is selected by specifying standard cylinders with standard rod diameters and using them at or below the rated pressure.

For long stroke cylinders under compressive loads, the use of stop tubes should be considered, to reduce bearing stress. The Piston Rod Selection Chart in this catalog provides guidance where unusually long strokes are required.

Parker Hannifin Corporation
Cylinder Division
Des Plaines, Illinois USA

Figure D.3: Report of the chosen hydraulic cylinder

Parker Hannifin Cylinder Configurator ™

Summary Report

Model Code, for info only : 63BBHMIRNS24M620.00M1102

Product Summary

Part Number	HMI-220626130504516
Bore	63 mm
Mounting Style	BB - Cap Fixed Clevis (ISO Style MP1)
Port	R - ISO 1179-1(BSPP) - G1/2
Piston	N - Standard Piston
Head End - Rod No	2- 45 mm
Head End - Piston Rod End	4 - Male thread
Head End - Rod Thread	M - M20x1.5
Stroke	620.00
Fluid medium	M - Group 1 Mineral Oil HH, HL, HLP, HLP-D, HM, HV, MIL-H-5606 Oil, Air, Nitrogen
Ports Position Head	1
Ports Position Cap	1
Air Bleeds Head	None
Air Bleeds Cap	2
Stop Tube length	50.00
End of Stroke Switch: Position Head	2
End of Stroke Switch: Position Cap	2
Eye Bracket BB Mtg.	144812
Eye Bracket BB Mtg. Qty	1.0
Rod Clevis	143453
Rod Clevis Qty	1.0
Plain Rod Eye	143463

6/26/2022 1:13:32 PM 1

Appendix E

Power Unit

E.1 Tank

Figure E.1: Available tanks [36]

BUCHER hydraulics

3.1.3 Square plastic tanks from 1 to 4 litres

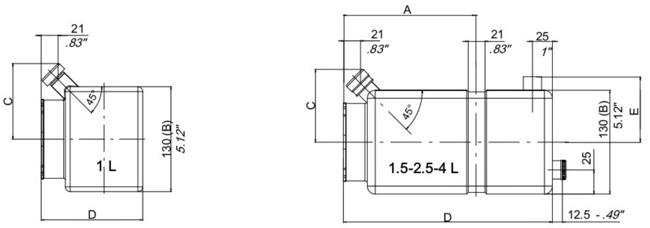

Nom capacity		Type	Code	Fixing Position	A		B		C		D		E	
Litres	*U.S.G .P.M.*				mm	inch	mm	inch	mm	inch	mm	inch	mm	inch
1	*0.26*	P-010Q-A	200973220030	P01-P02-P03-P04 P05-P15-P25-P35	-				99	*3.9*	126	*4.96*		
1.5	*0.40*	P-015Q-A	200973230030		-				99	*3.9*	159	*6.26*		
1.5	*0.40*	P-015Q-E	200973230070		-				99	*3.9*	159	*6.26*		
1.5	*0.40*	P-015Q-D	200973230060	P01-P02-P03-P04	-				99	*3.9*	159	*6.26*		
1.5	*0.40*	P-015Q-B	200973230040		-				99	*3.9*	159	*6.26*		
1.5	*0.40*	P-015Q-F	200973230080		-				99	*3.9*	159	*6.26*		
2.5	*0.66*	P-025Q-A	200973240020	P01-P02-P03-P04 P05-P15-P25-P35	167	*6.6*			99	*3.9*	262	*10.3*		
2.5	*0.66*	P-025Q-E	200973240060		167	*6.6*			99	*3.9*	262	*10.3*		
2.5	*0.66*	P-025Q-D	200973240050	P01-P02-P03-P04	167	*6.6*	130	5.12	99	*3.9*	262	*10.3*	82	*3.23*
2.5	*0.66*	P-025Q-B	200973240030		167	*6.6*			99	*3.9*	262	*10.3*		
2.5	*0.66*	P-025Q-F	200973240070		167	*6.6*			99	*3.9*	262	*10.3*		
4.0	*1.05*	P-040Q-A	200973260020	P01-P02-P03-P04 P05-P15-P25-P35	232	*9.13*			99	*3.9*	327	*12.9*		
4.0	*1.05*	P-040Q-E	200973260060		232	*9.13*			99	*3.9*	327	*12.9*		
4.0	*1.05*	P-040Q-D	200973260050	P01-P02-P03-P04	232	*9.13*			99	*3.9*	327	*12.9*		
4.0	*1.05*	P-040Q-B	200973260030		232	*9.13*			99	*3.9*	327	*12.9*		
4.0	*1.05*	P-040Q-F	200973260070		232	*9.13*			99	*3.9*	327	*12.9*		

Horizontal and vertical mounting

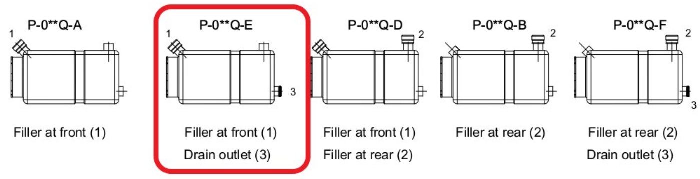

20/80 200-P-991186-EN-09/11.2019 UP50

E.2 Fixing Position

Figure E.2: Available fixing positions [36]

BUCHER hydraulics

3.2 Fitment and fixing positions

3.2.1 Fixing position: Horizontal

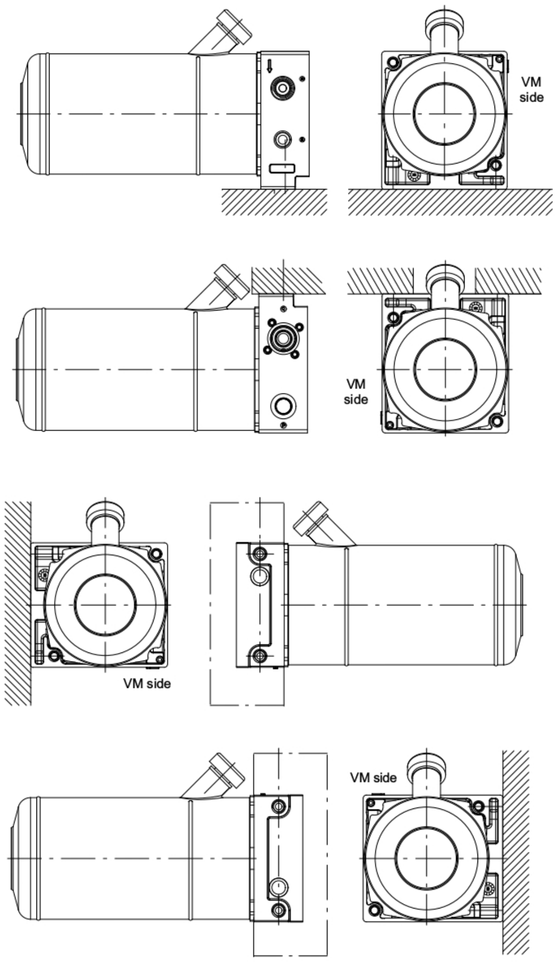

Assembling position P01

Assembling position P02

Assembling position P03

Assembling position P04

Example

	Tank														Fitting					Pos.		
3	P	0	1	0	R	-	A													P	0	1

E.3 Gear Pump

Figure E.3: Available reversible gear pumps [36]

BUCHER hydraulics

2.3 Gear pumps APR05/** -339F - Reversible

APR05/**-339F

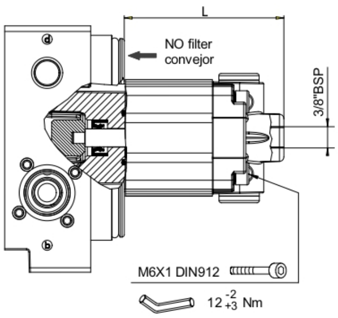

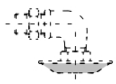

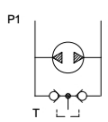

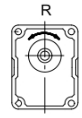

Reversible rotation

Example / Pump / Series

2 | A P R 0 5 / 0 , 5 | - 3 3 9 F

AP05	Displace-ment		Order code	L		Max. pressure						n. min.		n. max.
Pump type	cm^3/rev	Cu.In. P.R		mm	inch.	P1 bar	P1 PSI	P2 bar	P2 PSI	P3 bar	P3 PSI	P<100 bar	P>100 bar	P>P1
APR05/0.25-339F	0.25	.015	200748120180	63	2.48	150	2170	160	2320	180	2610	800	3000	7000
APR05/0.5-339F	0.5	.030	200748130165	65	2.56	170	2460	190	2750	210	3040	650	3000	7000
APR05/0.75-339F	0.75	.045	200748140100	67	2.64	170	2460	190	2750	210	3040	650	1500	7000
APR05/0.9-339F	0.9	.055	200748150100	68.5	2.69	170	2460	190	2750	210	3040	650	1500	7000
APR05/1.2-339F	1.2	.075	200748160210	71	2.79	150	2170	160	2320	180	2610	550	1500	6000
APR05/1.6-339F	1.6	.10	200748180110	74.7	2.94	150	2170	160	2320	180	2610	550	1500	6000
APR05/2.3-339F	2.3	.140	200748190060	80.6	3.17	130	1880	140	2030	160	2320	550	1500	4500

18/80

200-P-991186-EN-09/11.2019
UP50

E.4 A.C. Motors

Figure E.4: Available A.C. Motors - part 1 [36]

BUCHER hydraulics

5.2.2 Standard interface (flange/drive needed)

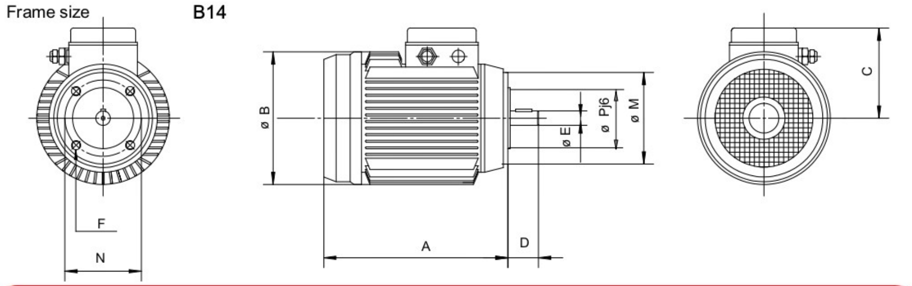

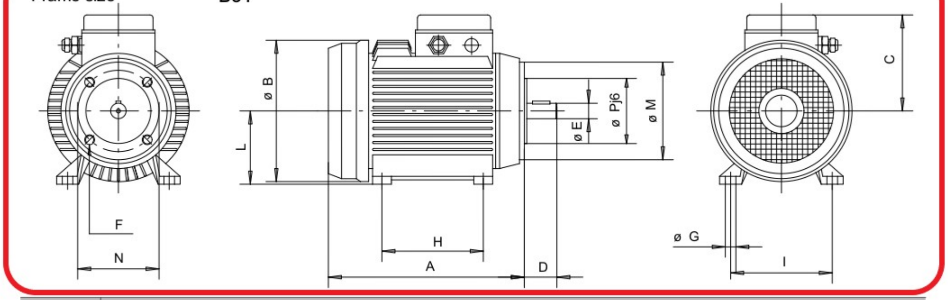

Size	Units	A	B	C	D	E	F	G	H	I	L	M	N	P
		Dimensions												
63	mm	189	124	104	23	11	M5	7	80	100	63	90	75	60
	inch	7.44	4.88	4.09	.90	.43		.28	3.14	3.93	2.48	3.54	2.95	2.36
71	mm	218	140	109	30	14	M6	7	90	112	71	105	85	70
	inch	8.58	5.51	4.29	1.18	0.55		0.27	3.54	4.41	2.79	4.13	3.35	2.76
80	mm	237	156	123	40	19	M6	9	100	125	80	120	100	80
	inch	9.33	6.14	4.84	1.57	0.75		0.35	3.94	4.92	3.15	4.72	3.94	3.15

5.2.3 Standard interface 4 pole - 50 Hz - 230 V

Frame size B14 SINGLE PHASE motor				
Power kW	Power HP	Size	Type	Code
0.12	0.16	63	T211	200543160411
0.18	0.25	63	T212	200543160811
0.25	0.33	71	T209	200543161221
0.37	0.5	71	T201	200543161823
0.55	0.75	80	T202	200543162231
0.75	1	80	T203	200543162631

Frame size B34 SINGLE PHASE motor				
Power kW	Power HP	Size	Type	Code
0.12	0.16	63	T711	200543160412
0.18	0.25	63	T712	200543160812
0.25	0.33	71	T709	200543161223
0.37	0.5	71	T701	200543161822
0.55	0.75	80	T702	200543162233
0.75	1	80	T703	200543162633

Figure E.5: Available A.C. Motors - part 2 [36]

BUCHER hydraulics

5.2.4 Standard interface 4 pole - 50 Hz - S1 - 230/400 V

Frame size B14 THREE PHASE motor					
	Power		Size	Type	Code
	kW	HP			
	0.12	0.16	63	**T011**	200543560411
	0.18	0.25	63	**T012**	200543561041
	0.25	0.33	71	**T009**	200543561221
	0.37	0.5	71	**T001**	200543561821
	0.55	0.75	80	**T002**	200543562231

Frame size B34 THREE PHASE motor					
	Power		Size	Type	Code
	kW	HP			
	0.12	0.16	63	**T511**	200543560442
	0.18	0.25	63	**T512**	200543561011
	0.25	0.33	71	**T509**	200543561222
	0.37	0.5	71	**T501**	200543561824
	0.55	0.75	80	**T502**	200543562232

5.2.5 Standard interface 4 pole - 50 Hz - S3=70% - 230/400 V

Frame size B14 THREE PHASE				
Power		Size	Type	Code
kW	HP			
0.75	1	80	**T003**	200543562631

Frame size B34 THREE PHASE				
Power		Size	Type	Code
kW	HP			
0.75	1	80	**T503**	200543562632

5.2.6 Mounting position

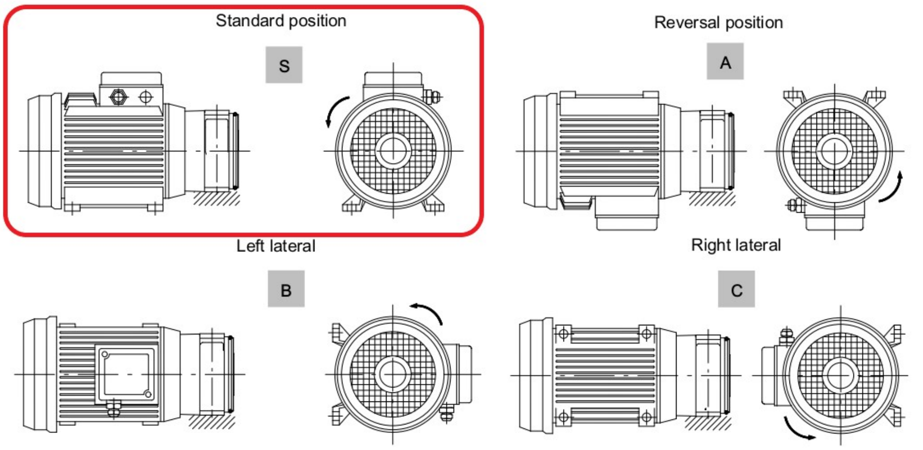

Example	Electric motor	Pos	Relay	Pos
5	T 5 0 3	S		

N.B.: Looking at the fan side the e. motor must rotate counterclockwise

42/80

200-P-991186-EN-09/11.2019
UP50

E.5 Pressure Relief Valves

Figure E.6: Available pressure relief valves [36]

BUCHER
hydraulics

7.2 Pressure relief valves

7.2.1 Pressure relief valve: **VM01

Direct acting
Balanced piston
Adjustable setting
Three setting ranges

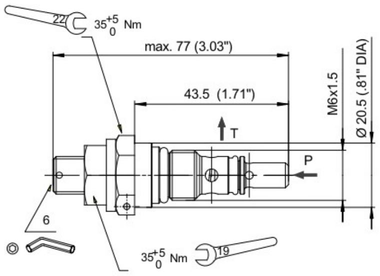

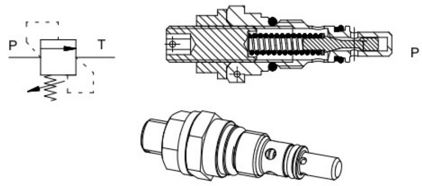

The valve can be sealed against tampering.

Option: sheath shrink tamperature: T=60°
CAP02 code 200660200031

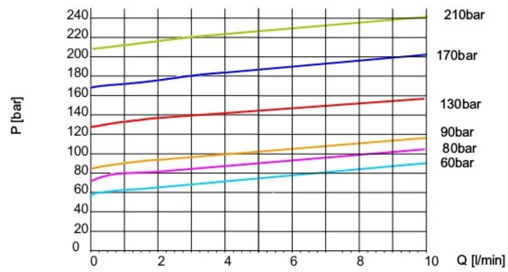

The purpose of a relief valve is to keep the maximum system pressure at a safe level. When the hydraulic power unit is supplied with pressure relief valves, the correct calibration is provided by Bucher Hydraulics S.p.A. and there are no reasons to change this value.
When ordering, state in full the sheath part number, and, if the valve is to be supplied with sheath already fitted, the relief pressure setting required.
*** Maximum admitted pressure value: 210 bar when used into the diecast alluminium alloy body
Pressure setting
For present values other than those indicated, replace the first two digits of the designation with the setting required. For example, required setting 130 bar: designation type 13VM01. Always check that the required value falls within the standard ranges of adjustment

Performances	
Max. Flow rate	7 l/min.
Max. Pressure	210 bar
Weight	0.0852 kg
Oil viscosity	12 to 400 cSt
Oil temperature	-20 to 100 °C
Recomanded filtration	21/19/16 (10 NAS 1638)

Spring	Setting range	Standard setting	Type	Code
00	Plug	No valve	**00VC00**	200778400200
03	5 - 40 bar	30 bar	**03VM01**	200787400840
06	45 - 80 bar	60 bar	**06VM01**	200787400850
15	85 - 210 bar	150 bar	**15VM01**	200787400860

50/80

200-P-991186-EN-09/11.2019
UP50

E.6 Power Pack Housing

Figure E.7: Power pack housing - Model K50 [36]

BUCHER
hydraulics

1.4 Housing UP50K50-K52 (Reversible circuit) with threaded ports

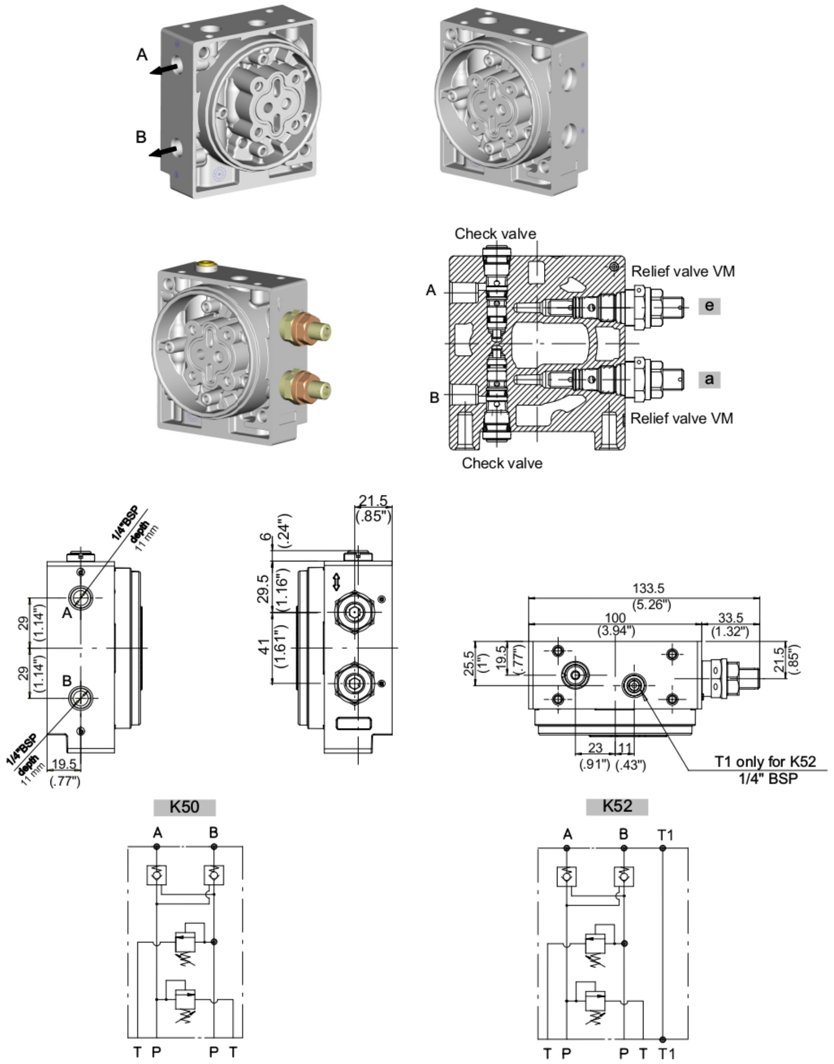

Type	Port A	Port B
UP50K50	1/4" BSP	1/4" BSP

Type	Port A	Port B	Port T1
UP50K52	1/4" BSP	1/4" BSP	1/4" BSP

200-P-991186-EN-09/11.2019
UP50
13/80

E.7 Drives

Figure E.8: Drives for A.C. motors [36]

BUCHER hydraulics

6.3 Drives for D.C. motors

The tables allow selection to select the correct drive in function of the selected motor.

Motor type		Voltage	Power	Type
C120PD/C0		12 V	500W	E61
C220PD/C0		24 V	500W	
C128PK/A0	C134AK/O0 + R109	12 V	800W	
C228PK/A0	C228PK/A0 + R215	24 V	800W	
C134AK/O0	C134AK/O0 + R109	12 V	1500W	E65
C238AK/P0	C238AK/P0 + R215	24 V	2000 W	
T82K		48 V	2000 W	
C135AB/H0	C135AB/H0 + R109	12 V	1600W	E66
C240AB/S0	C240AB/S0 + R215	24 V	2200 W	

6.4 Drives for A.C. motors

6.4.1 Single phase

Motor type	Power		Size	Drive
	kW	HP		
T211-T711	0.12	0.16	63	E30
T212-T712	0.18	0.25		
T209-T709	0.25	0.33	71	E33
T201-T701	0.37	0.5		
T202-T702	0.55	0.75	80	E31
T203-T703	0.75	1		

6.4.2 Three phase

Motor type	Power		Size	Drive
	kW	HP		
T011-T511	0.12	0.16	63	E30
T012-T512	0.18	0.25		
T009-T509	0.25	0.33	71	E33
T001-T501	0.37	0.5		
T002-T502	0.55	0.75	80	E31
T003-T503	0.75	1		

44/80

200-P-991186-EN-09/11.2019
UP50

Figure E.9: Drive E31 [36]

BUCHER
hydraulics

6.8 Drive E30

Code E30 200960400040

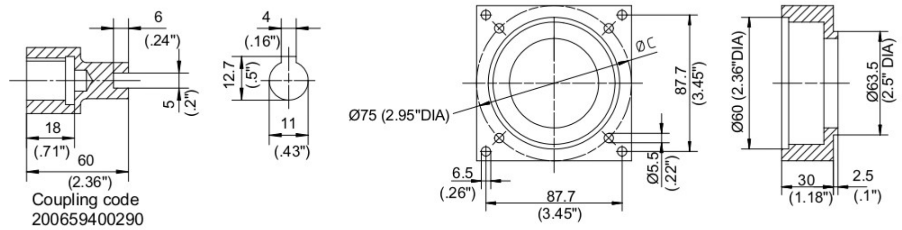

6.9 Drive E31

Code E31 200960400050

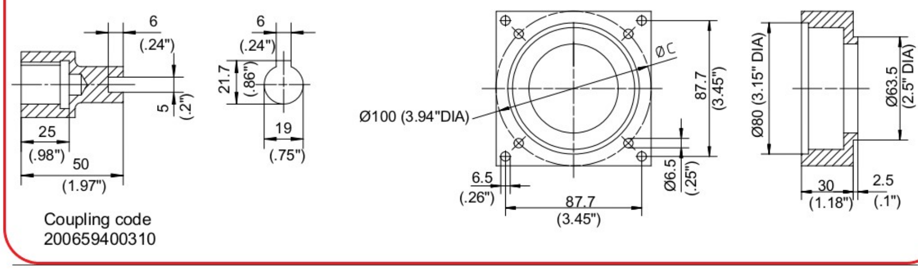

6.10 Drive E33

Code E33 200960400060

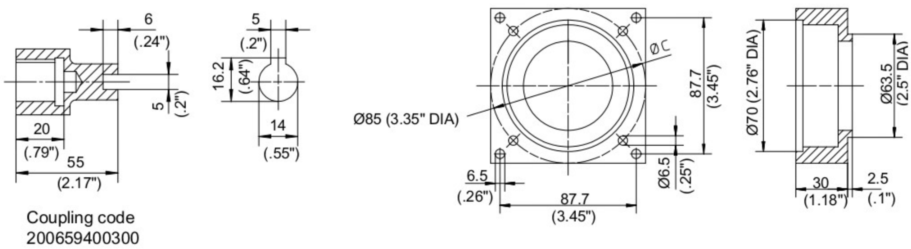

E.8 Solenoid Valve

Figure E.10: Solenoid operated directional valve: SPD817/22-TV [36]

BUCHER hydraulics

7.3.1 Solenoid operated directional valve: SPD817/22-TV

Normally closed
Piloted - 16 W
Poppet type
Flow from 1 to 2

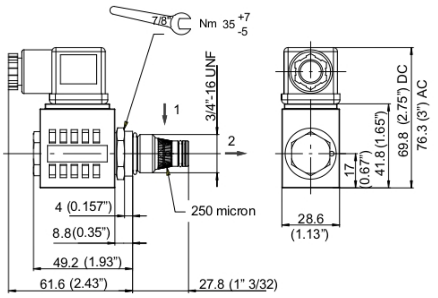

Weight (complete valve): 0.230 Kg

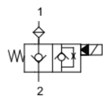

Performances	
Max. pressure (***)	270 bar
Max. recommended pressure	See 2.2
Max. flow	20 l/min.
Rated power	16 Watt
Intermittence	ED= 100%
Voltage tolerance	± 10%
Internal leakage	0-5 drops/min.
Temperature range	-20/+90 °C
Connector type	DIN 43650
Time to open 12 V 20 l/min 80% of final change of state	16 ms.
Time to close 12 V - 20 l/min 80% of final change of state	18 ms.
O-Ring replacement kit	200974200480

*** = max.admitted pressure when used into power pack bodies: 230 bar

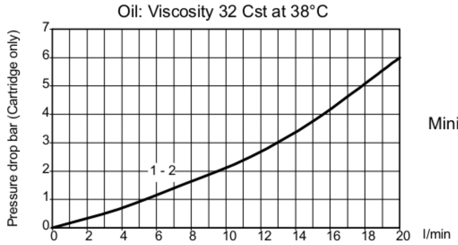

Minimum suggested working pressure = 5 bar

Directional valve without coil and connector

Type	Code*
SPD817/22-TV P.M.	200533910019

* Mechanical part code only. For connector and coil see section: 7.3.5 - 7.3.6

E.9 Mechanical Valve

Figure E.11: Piloted check valve: VRP05 [36]

BUCHER hydraulics

7.4 Mechanical valves

7.4.1 Check valve: VR05

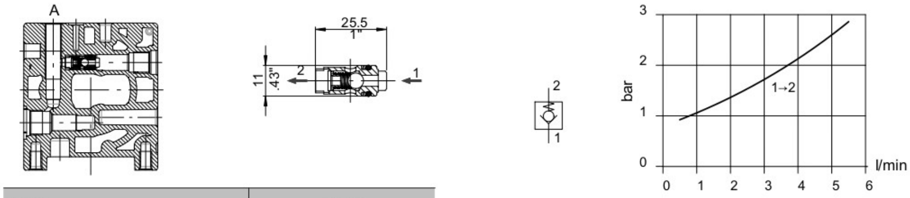

Type	Code
VR05	200787601330

7.4.2 Piloted check valve: VRP05

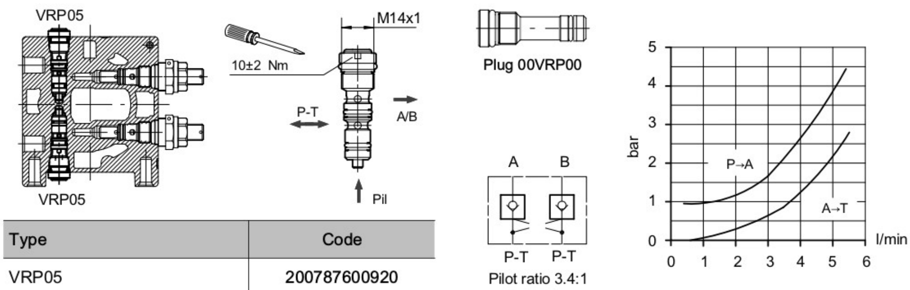

Type	Code
VRP05	200787600920
00VRP00	200778400430

To be assembled in K50 - K51 housings only

7.4.3 Throttle compensated flow control valve: VRC05

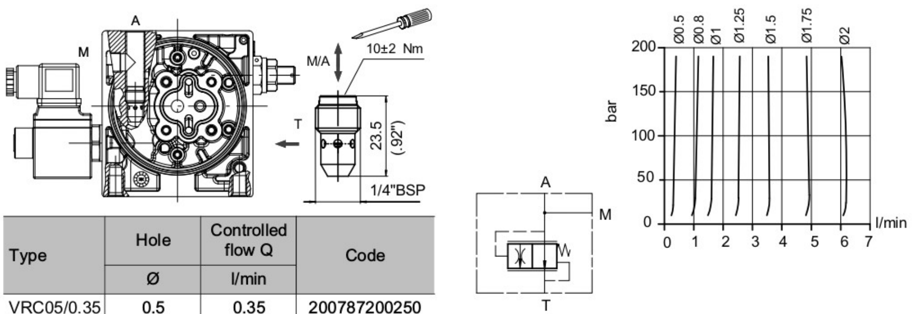

To be assembled in K04 - K41 housing only

Type	Hole	Controlled flow Q	Code
	Ø	l/min	
VRC05/0.35	0.5	0.35	200787200250
VRC05/1	0.8	1	200787200260
VRC05/1.6	1	1.6	200787200270
VRC05/2.5	1.25	2.5	200787200280
VRC05/3.5	1.5	3.5	200787200290
VRC05/4.9	1.75	4.9	200787200300
VRC05/6	2	6	200787200310

Flow tolerance = ±15%

Appendix F

Pillow Block - P 20 RM

Figure F.1: Technical specifications of pillow block P 20 RM - part 1 [40]

SKF. Generated from www.skf.com on 2022-06-18

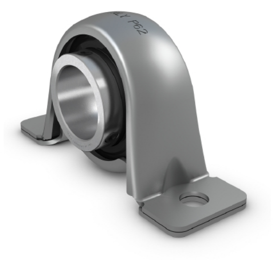

P 20 RM

Pillow block ball bearing units

The values depend on the included bearing:
table 1, table 2, table 3,
table 4

Technical specification

Compliance with standard	ISO*
Purpose specific	For material handling applications
Housing material	Pressed steel
Sealing solution	Standard seals

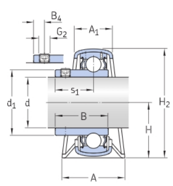

DIMENSIONS

d	20 mm	Bore diameter
d_1	≈ 28.2 mm	Shoulder diameter inner ring
A	32 mm	Base width
A_1	21 mm	Top width
B	25.5 mm	Width of inner ring
B4	4.5 mm	Distance from locking device side face to thread centre
H	25.3 mm	Height of spherical seat centre
H_1	3 mm	Foot height
H_2	50.5 mm	Overall height
J	76 mm	Distance between attachment bolts
L	98.5 mm	Overall length
N	9.6 mm	Diameter of attachment bolt hole

SKF. Page 1 of 4

Figure F.2: Technical specifications of pillow block P 20 RM - part 2 [40]

SKF. Generated from www.skf.com on 2022-06-18

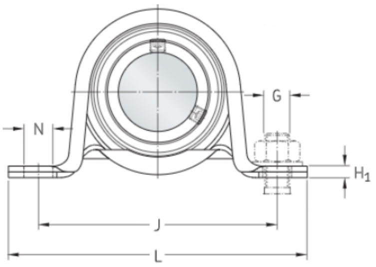

s1	18.3 mm	Distance from locking device side face to raceway centre

CALCULATION DATA

Basic dynamic load rating	C	12.7 kN
Basic static load rating	C_0	6.55 kN
Fatigue load limit	P_u	0.28 kN
Permissible radial housing load		max. 1.7 kN
Limiting speed		8 500 r/min
with shaft tolerance h6		

MASS

Mass bearing unit	0.22 kg

MOUNTING INFORMATION

Set screw	G_2	M6x0.75
Hexagonal key size for set screw		3 mm
Recommended tightening torque for set screw		4 Nm
Recommended diameter for attachment bolts, mm	G	8 mm
Recommended diameter for attachment bolts, inch	G	0.313 in

INCLUDED PRODUCTS

Appendix G

Leveling Foot

Figure G.1: Datasheet of the chosen leveling feet - part 1 [41]

27794 Pés niveladores redondos norelem

Descrição do artigo/Imagens dos produtos

Descrição

Material:
Poliamida.
Parafuso em aço.

Versão:
preto.
Parafuso galvanizado.

Indicação:
Pé nivelador com fenda cruzada em base de prato como suporte de montagem.
Versão rígida.

Desenhos

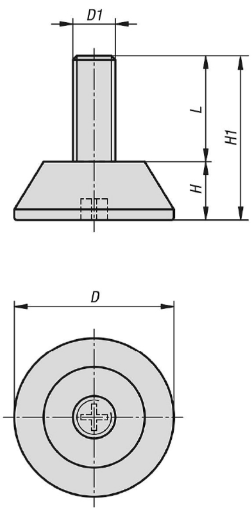

Visão geral dos artigos

Código do artigo	D	D1	H	H1	L	Capacidade de carga máx. kN (apenas com carga estática)
27794-3006X020	30	M6	11	31	20	3
27794-3006X030	30	M6	11	41	30	3
27794-3008X016	30	M8	11	27	16	3

© norelem www.norelem.com 1/2

Figure G.2: Datasheet of the chosen leveling feet - part 2 [41]

27794 Pés niveladores redondos

norelem

Visão geral dos artigos

Código do artigo	D	D1	H	H1	L	Capacidade de carga máx. kN (apenas com carga estática)
27794-3008X020	30	M8	11	31	20	3
27794-3008X025	30	M8	11	36	25	3
27794-3008X030	30	M8	11	41	30	3
27794-3008X040	30	M8	11	51	40	3
27794-3010X025	30	M10	11	36	25	3
27794-3010X030	30	M10	11	41	30	3
27794-3010X035	30	M10	11	46	35	3
27794-4708X016	47	M8	11	27	16	4
27794-4708X020	47	M8	11	31	20	4
27794-4708X030	47	M8	11	41	30	4
27794-4708X040	47	M8	11	51	40	4
27794-4710X020	47	M10	11	31	20	4
27794-4710X030	47	M10	11	41	30	4
27794-4710X055	47	M10	11	66	55	4